이학석사학위논문

Higher-order band topology in two-dimensional lattices

2차원 격자의 고차 위상 띠 이론

2020 년 2 월

서울대학교 대학원

물리천문학부

이 은 우

Higher-order band topology in two-dimensional lattices

2차원 격자의 고차 위상 띠 이론

지도교수 양 범 정

이 논문을 이학석사 학위논문으로 제출함

2020 년 1 월

서울대학교 대학원

물리천문학부 물리학전공

이 은 우

이은우의 이학석사 학위논문을 인준함

2020 년 1 월

위 원 장 _____ (인)

부위원장 _____ (인)

위 원 _____ (인)

Abstract

Bulk-boundary correspondence is the fundamental property of topological phases. In conventional topological insulators, the gapped bulk states in d-dimensions support metallic states in $(d-1)$-dimensional surfaces. Recently, however, a class of topological crystalline insulators violating the conventional bulk-boundary correspondence has been proposed, and they are nowadays called higher-order topological insulators (HOTIs). In contrast to the conventional topological insulators, the gapless excitations of a HOTI in d-dimensions are localized in a subspace with a dimension lower than $(d-1)$, such as corners or hinges, when the global shape of the material preserves the crystalline symmetry relevant to the nontrivial bulk band topology. In the thesis, we investigate novel properties that can appear in 2D higher-order insulators protected by crystalline symmetries.

First, we show that the band topology of graphene with a Kekule texture is a 2D second-order insulator characterized by the 2D $\mathbb{Z}_2$ topological invariant w_2, which is quantized in systems with inversion symmetry. Also, we propose monolayer graphdiyne (MGD) as the first realistic candidate material for 2D HOTIs protected by inversion symmetry which has same crystalline symmetries as Kekule textured graphene. We show that, despite the absence of chiral symmetry, the higher-order topology of MGD is manifested in the filling anomaly and charge accumulation at two corners. Interestingly, although its low-energy band structure can be properly described by using only p_z orbital basis, the higher-order topology itself originates from the core electronic orbitals. We also show that the higher-order topology of MGD is the fun-

damental origin of the nontrivial band topology of ABC-stacked graphdiyne hosting monopole nodal lines and hinge states.

Second, we establish the correspondence between the fractional charge bound to a vortex in textured lattice and the relevant bulk band topology in two-dimensional (2D) HOTIs. The fractional charge localized at a vortex in the Kekule texture is shown to be related to the change in the bulk topological invariant w_2 around the vortex, as in the case of the Su-Schriefer-Heeger model in which the fractional charge localized at a domain wall is related to the change in the bulk charge polarization between degenerate ground states. We show that the effective three-dimensional (3D) Hamiltonian, where the angle θ around a vortex in Kekule-textured graphene is a third coordinate, describes a 3D axion insulator with a quantized magnetoelectric polarization. The spectral flow during the adiabatic variation of θ corresponds to the chiral hinge modes of an axion insulator and determines the accumulated charge localized at the vortex. For the cases when magnetoelectric polarization is quantized due to the presence of symmetry that reverses the space-time orientation, we classify all possible topological crystalline insulators whose vortex defect carries a fractional electric charge.

Keywords: higher-order topology, crystalline symmetry, monolayer graphdiyne, topological vortex

Student Number: 2017-24557

Contents

Chapter 1

Introduction

The thesis is organized as follows. In this chapter, we review topological insulators in 1D and 2D and the corresponding topological invariants. The relation between the topological invariants and bulk-boundary correspondence is also discussed. In chapter 2, we briefly introduce topological invariants in inversion symmetric 2D higher-order topological insulators (HOTIs). Then, we propose Kekule graphene and monolayer graphdiyne as the realistic materials that reveal higher-order topology protected by inversion symmetry. In chapter 3, we show how the charge fractionalization in a vortex in 2D Kekule textured graphene is related to its bulk band topology. Generalizing the relationship, we classify all topological crystalline vortices that carry a fractional charge. Finally, we provide conclusions. Let us note that the contents of the paper overlap with two papers uploaded to arXiv: arXiv1903.02737 and arXiv 1904.11452.

1.1 Charge fractionalization in SSH model

In topological band theory, one studies non-interacting Hamiltonians that are invariant under translation symmetry. In such systems, the Bloch theorem is applied as follows

$$\Psi_{\mathbf{k}}(\mathbf{x}+\mathbf{a}) = e^{i\mathbf{k}\cdot\mathbf{a}}\Psi_{\mathbf{k}}(\mathbf{x}), \tag{1.1}$$

where $\Psi_{\mathbf{k}}(\mathbf{x})$ is the Bloch wave-function with momentum $\mathbf{k}$ that satisfies the Schrodinger equation $H\Psi_{\mathbf{k}}(\mathbf{x}) = E_{\mathbf{k}}\Psi_{\mathbf{k}}(\mathbf{x})$, and $\mathbf{a}$ is multiples of the lattice vector. Due to the theorem, one can construct Brillouin zone that has torus geometry $k_i \sim k_i + 2\pi$.

Here let us review the physics of charge fractionalization described by the Su-Schriefer-Heeger (SSH) model [1]. The Hamiltonian can be written as

$$H_{\mathrm{SSH}} = \sum (t + \delta t_i) a_i^\dagger a_{i+1} + H.c \tag{1.2}$$

where t is the hopping amplitude, and its modulation is described by $\delta t_i = (-1)^i \Delta$. Also, we assume that the system is half-filled. If Δ is 0, the energy dispersion is gapless and the unit cell contains one atom. However, when Δ is non-zero constant, the nth unit cell contains $2n-1$ and $2n^{\mathrm{th}}$ atoms and the gapped band structure appears. The unit cell becomes doubled and the size of the Brillouin zone is reduced by half.

Spontaneous formation of lattice dimerization gives rise to two degenerate ground states distinguished by the opposite sign of the mass term Δ. At the boundary between two phases with the opposite mass term, there exists a localized zero-mode wave function and the bound charge is quantized into 1/2, which is the bulk-boundary correspondence of the SSH model. Let us introduce two approaches to show the existence of fractional bound charges.

In the first approach, we solve the low energy Dirac equation given by

$$H(x) = \begin{pmatrix} -i\partial_x & \Delta(x) \\ \bar{\Delta}(x) & i\partial_x \end{pmatrix}. \tag{1.3}$$

At the domain wall, $\Delta(x)$ changes from -Δ_0 to Δ_0. The equation satisfied by the zero-mode solution is $H(x)\psi(x) = 0$ where $\psi(x) = (u(x), v(x))^T$. More explicitly,

$$\begin{aligned} -i\partial_x u(x) + \Delta(x)v(x) = 0, \\ \bar{\Delta}(x)u(x) + i\partial_x v(x) = 0. \end{aligned} \tag{1.4}$$

Under the solitonic mass background, one can find a normalizable zero energy wave function $\psi(x) \sim e^{-\int_0^x |\Delta(x')|dx'}$, which gives a half electric charge localized at the domain wall.

In the second approach, one can explain the existence of fractional charge in terms of the bulk topological property. In 1D systems, topological invariant is defined as polarization P_1, which is expressed as

$$P_1 \equiv \frac{1}{2\pi} \oint A(k)dk \mod 1, \tag{1.5}$$

where $A(k) = -i\langle n(k)|\partial_k|n(k)\rangle$ is Berry connection, and $|n(k)\rangle$ is an eigenstate of the Hamiltonian $H(k)$ with energy $\mathcal{E}(k)$. In the presence of inversion I or chiral S symmetry, P is quantized into 0 or 1/2 mod 1. In the SSH model, the Hamiltonian possesses both inversion and chiral symmetry, so that P_1 is quantized to 0 (1/2) modulo 1 for trivial (topological) phase. In our convention, $\Delta > 0$ corresponds to the topological phase and $\Delta < 0$ corresponds to the trivial phase. The invariant is determined by the parity eigenvalues at the time-reversal invariant momentum (TRIM) points as [2, 3]

$$(-1)^{P_1} = (-1)^{N_{\rm occ}^-(k=0)}(-1)^{N_{\rm occ}^-(k=\pi)} \tag{1.6}$$

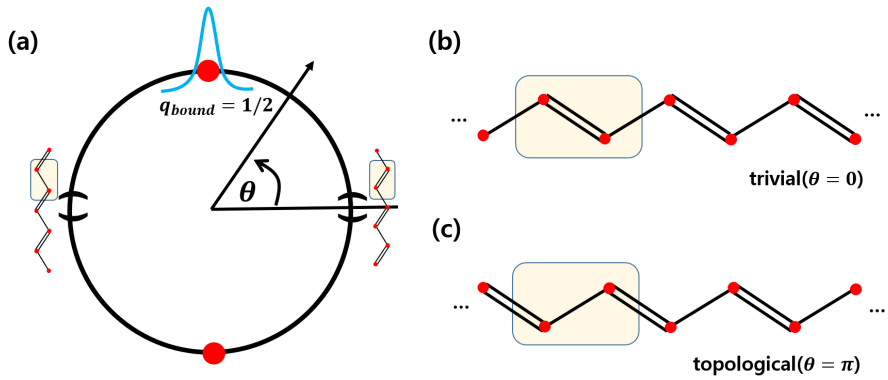

Figure 1.1 (Color online) (a) An adiabatic cycle interpolating two insulators with the charge polarization $P_1 = 0$ and $P_1 = 1/2$, respectively. (b) Schematic figures describing the trivial (topological) phase with the parameter $\theta = 0$ ($\theta = \pi$)

where $N^-_{\rm occ}(\Gamma_i)$ is the number of occupied states with negative parity at Γ_i. The bound charge between two insulators with $P_1 = 0$ and $P_1 = 1/2$ is expressed by the integral of the polarization gradient

$$q_{\rm bound} = \int -\partial_x P_1 dx = 1/2 \text{ mod } 1, \tag{1.7}$$

which indicates the half integral electric charge localized at the domain wall.

1.1.1 Wilson loop and polarization

In general, number of occupied bands is bigger than one. If occupied bands are separable to single band, the total polarization is $\sum_{n=1}^{n_{occ}} P_1^n$ where $n_{\rm occ}$ is number of occupied bands. However, if the bands are not seperable due to symmetry constraints, one must consider the non-Abelian extension of polarization: Wilson loop. Wilson loop is a gauge-invariant observable whose eigenvalue spectrum contains the information on the topological properties of

the Hamiltonian. Wilson loop operator is defined by

$$\begin{aligned} W_{(k_1+2\pi,k_2)\leftarrow(k_1,k_2)} &\equiv W_{x,\mathbf{k}} \\ &= \lim_{N\to\infty} F_{N-1}F_{N-2}\cdots F_1F_0 \\ &= Pe^{-i\oint_C A_k dk}, \end{aligned} \tag{1.8}$$

where $[F_i]_{nm} = \langle u_m(k_{i+1},k_2)|u_n(k_i,k_2)\rangle, k_i = \frac{2\pi}{N}i$ and $m,n = 1,\cdots,n_{occ}$. Since a Wilson loop operator is unitary, the eigenvalue equation is given by $W_{x,\mathbf{k}}|\nu^j_{x,\mathbf{k}}\rangle = e^{i\nu^j_x(k_y)}|\nu^j_{x,\mathbf{k}}\rangle$, where $\nu^j_x(k_y)$ corresponds to x-component of Wannier center of jth Wannier functions. It follows that the electron charge polarization is expressed as $P_{1,x} = \frac{1}{2\pi N_y}\sum_{k_y}\sum_j \nu^j_x(k_y) = -\frac{i}{2\pi}\log\det[W_{x,\mathbf{k}}]$. In the presence of P symmetry, the set of eigenvalues satisfy $\{\nu_x(k_y)\} \equiv \{-\nu_x(-k_y)\}$ mod 2π, so that the polarization is quantized into either 0 or $1/2$ modulo 1.

1.2 Chern Insulator

So far, we have described 1D topological invariant that is given by the integral of Berry phase: polarization or Wilson loop spectrum. Note that Berry phase itself is not gauge invariant since $A(\mathbf{k}) \to A(\mathbf{k}) - \nabla_k\alpha(\mathbf{k})$ as $|u(\mathbf{k})\rangle \to e^{i\alpha(\mathbf{k})}|u(\mathbf{k})\rangle$. In 2D, one can define gauge-invariant observable, Berry curvature $\Omega(\mathbf{k}) = \frac{\partial}{\partial k_x}A_y(\mathbf{k}) - \frac{\partial}{\partial k_y}A_x(\mathbf{k}) = \nabla_{\mathbf{k}}\times\mathbf{A(k)}$. The surface integral of the Berry curvature $-\frac{1}{2\pi}\int\Omega(\mathbf{k})dk_xdk_y$ is quantized into integer, which is called Chern number. If an insulator has a non-zero Chern number, it is called the Chern insulator. Chern insulator is similar to integer quantum Hall insulator in a sense that they both have dissipationless chiral edge modes. The only difference is the absence/existence of an external magnetic field.

In the presence of P symmetry, Chern number C is related to the difference of polarization defined on time reversal invariant momentum (TRIM) points

$k_y = 0$ and $k_y = \pi$:

$$(-1)^C = (-1)^{(P(k_y=\pi)-P(k_y=0))}, P_{k_y} = \frac{1}{2\pi}\int_{k_x=0}^{2\pi} dk_x A(k_x, k_y). \tag{1.9}$$

In other words, Chern insulator can be thought of as a charge polarization pumping process between 1D topological and trivial insulators. Combining eqn. (1.6) and (1.9), the parity of Chern number is expressed by the inversion eigenvalues at TRIM points Γ_i.

$$(-1)^C = (-1)^{\sum N^-_{\rm occ}(\Gamma_i)}, \tag{1.10}$$

where $N^-_{\rm occ}(\Gamma_i)$ is the number of occupied states with negative parity at Γ_i [4].

The low-energy property of the inversion symmetric Chern insulator can be captured by 2×2 Dirac Hamiltonian. For convenience, let us consider a disk-shaped finite-size system with a circular boundary.

$$\begin{aligned} H(x,y) &= -iv_x\partial_x\sigma_x - iv_y\partial_y\sigma_y + M(r)\sigma_z. \\ &= -i\sigma_1(\theta)\partial_r - i\sigma_2(\theta)r^{-1}\partial_\theta + M(r)\sigma_z, \end{aligned} \tag{1.11}$$

where $\sigma_1(\theta) = \cos\theta\sigma_x + \sin\theta\sigma_y$ and $\sigma_2(\theta) = -\sin\theta\sigma_x + \cos\theta\sigma_y$. The inversion symmetry P can be expressed as σ_z, so that $PH(x,y)P^{-1} = H(-x,-y)$. The corresponding gapped insulator should be either a Chern insulator ($M > 0$) or a trivial insulator ($M < 0$) depending on the sign of the mass M. For a Chern insulator, $M > 0$ inside the bulk and $M < 0$ in a vacuum, where the mass term vanishes at the boundary and gapless chiral edge mode is observed. Employing a projection operator $\hat{P}(\theta) = \frac{1}{2}(1 + i\sigma_1(\theta)\sigma_z)$ at the boundary $r = R$,

$$H_{\rm edge}(x,y)|_{r=R} = -i\sigma_2(\theta)R^{-1}\partial_\theta. \tag{1.12}$$

1.3 2D Z_2 topological insulator

Moreover, there is another topological insulator in 2D that is time-reversal invariant, so-called 2D Z_2 TI. While Chern insulators have unidirectional gap-

less edge modes, Z_2 TIs have counter-propagating helical edge modes. Naively, Z_2 TI can be viewed as double copies of Chern insulators with opposite Chern numbers: $H_{Z_2} \cong H_{C=+1} \oplus H_{C=-1}$. Although the Chern number is zero, topolgocial invariant for Z_2 TI is given by the Fu-Kane formula. In the presence of inversion symmetry, in particular, it is expressed as

$$(-1)^{\nu_{2D}} = \prod_{i=1}^{4} (-1)^{N_{\rm occ}^{-}(\Gamma_i)/2}, \tag{1.13}$$

where $N_{\rm occ}^{-}(\Gamma_i)$ is the number of occupied states with negative parity at Γ_i. One can easily check that the invariant is also nontrivial for double copies of Chern insulators.

The low energy Hamiltonian for a 2D P symmetric Z_2 TI is expressed as

$$H(\mathbf{x}) = i\partial_x \tau_x \sigma_x + i\partial_y \tau_x \sigma_y + M\tau_z \sigma_0, \tag{1.14}$$

where Pauli matrices τ and σ represent orbital and spin degrees of freedom and time reversal symmetry is $T = i\sigma_y K$ satisfying $TH(\mathbf{x})T^{-1} = H(\mathbf{x})$. Also inversion symmetry is expressed as $P = \tau_z \sigma_0$. If $M > 0$, the parity eigenvalues of occupied states are $(-1, -1)$. If $M < 0$ the parity eigenvalues are $(+1, +1)$. Thus, the Fu-Kane index of two opposite mass signs should be different, and the corresponding gapped insulator should be either a Z_2 TI ($M > 0$) or a trivial insulator ($M < 0$) depending on the sign of the mass M [5]. The Hamiltonian describing the gapless surface of the QSHI at the surface with normal vector $\hat{y}$ is

$$\begin{aligned} H_0 &= v_F \int dx (\psi_R^\dagger i\partial_x \psi_R - \psi_L^\dagger i\partial_x \psi_L), \\ &= v_F \int dx \Psi^\dagger i\tilde{\sigma_z} \partial_x \Psi, \end{aligned} \tag{1.15}$$

where $\psi_{R/L}$ is the right/left moving states and $\Psi^\dagger = (\psi_R^\dagger, \psi_L^\dagger)$. If time-reversal symmetry is broken, gapless edge states are gapped due to the surface mass terms $m_1\tilde{\sigma_x}$ and $m_2\tilde{\sigma_y}$.

Chapter 2

2D higher-order TI

2.1 Inversion symmetric 2D higher-order TI

In conventional topological insulators, the gapped bulk states in d-dimensions support metallic states in $(d-1)$-dimensional surfaces. Such a conventional bulk-boundary correspondence, however, is violated in a class of topological crystalline insulators, so-called higher-order topological insulators (HOTIs). The gapless excitations of a HOTI in d-dimensions are localized, instead, in a subspace with a dimension lower than $(d-1)$, such as corners or hinges, when the global shape of the material preserves the crystalline symmetry relevant to the nontrivial band topology.

In particular, the 2D second-order TI protected by inversion symmetry has a pair of corner states. The second-order nature of the topological insulator protected by P can be understood as follows. As described before, the low-

energy Hamiltonian of P-symmetric Z_2 TI is expressed as

$$H = -i\Gamma_1(\theta)\partial_r - i\Gamma_2(\theta)r^{-1}\partial_\theta + M(r)\Gamma_3, \tag{2.1}$$

where $\{\Gamma_i, \Gamma_j\} = \delta_{ij}$ for $i, j \in (1, 2, 3, 4, 5)$, $\Gamma_1(\theta) = \cos\theta\Gamma_1 + \sin\theta\Gamma_2$, and $\Gamma_2(\theta) = -\sin\theta\Gamma_1 + \cos\theta\Gamma_2$. Inversion symmetry P is represented as Γ_3. Let us assume that $M > 0$ inside the insulator and $M < 0$ outside the insulator. Employing a projection operator $\hat{P}(\theta) = \frac{1}{2}(1 + i\Gamma_1(\theta)\Gamma_3)$, we get a gapless surface Hamiltonian $H|_{r=R} = -iR^{-1}\tilde{\sigma_z}\partial_\theta$, which is a characteristic of a QSHI. If T symmetry is broken but non-local P symmetry is protected, surface mass terms are allowed: $H_m = m_4(\mathbf{r})\Gamma_4 + m_5(\mathbf{r})\Gamma_5$. It is worth noting that time-reversal symmetry is local in real-space, so that surface mass terms that open surface gap are not allowed in the presence of T symmetry. Under P symmetry, mass terms change sign: $m_i(\mathbf{r}) = -m_i(-\mathbf{r})$. Since two masses do not vanish simultaneously in general, the system does not exhibit anomalous corner states. However, in the presence of chiral symmetry, for instance, $\Gamma_5 H\Gamma_5^{-1} = -H$, m_5 must vanish, so that P symmetric corner states appear where $m_4(\mathbf{r})$ is zero.

In general, a 2D P-symmetric spinless fermion system carries three Z_2 topological invariants, w_{1x}, w_{1y}, and w_2 [6]. In terms of the sewing matrix $G_{mn}(\mathbf{k}) = \langle u_{m\text{-}\mathbf{k}}|P|u_{n\mathbf{k}}\rangle$, w_{1a} $(a = x,\ y)$ is given by its 1D winding number as

$$w_{1a} = -\frac{i}{2}\oint_C \nabla_{\mathbf{k}_a} \log\det G(\mathbf{k}) \mod 2, \tag{2.2}$$

which is equivalent to the quantized Berry phase Φ_a, in a way that $\Phi_a = \pi w_{1a} \pmod{2\pi}$ [7, 8]. w_{1a} can be determined by using relation $(-1)^{w_{1a}} = \prod_{i=1}^{2}(-1)^{N^-_{\rm occ}(\Gamma_i)}$, where $N^-_{\rm occ}(\Gamma_i)$ $(i = 1,\ 2)$ is occupied states with negative parity at Γ_i, and Γ_{1a}, Γ_{2a} are two TRIMs along the reciprocal lattice vector G_a. Since w_{1a} is equivalent to the quantized charge polarization along the G_a direction, it can be considered as a 1D topological invariant.

On the other hand, w_2 is a 2D topological invariant given by the 2D winding number of the sewing matrix $G(\mathbf{k})$ (modulo 2) [6], and measures the higher-order band topology of P-symmetric spinless fermion systems [9–11]. w_2 can be determined by

$$(-1)^{w_2} = \prod_{i=1}^{4} (-1)^{[N_{\rm occ}^{-}(\Gamma_i)/2]}, \tag{2.3}$$

where $N_{\rm occ}^{-}(\Gamma_i)$ is the number of occupied bands with odd parity at the TRIM Γ_i and the square bracket $[\alpha]$ indicates the greatest integer value of α [2, 3, 12–15]. Note that the index is the same as the Fu-Kane index for inversion symmetric Z_2 TI.

2.2 Kekule graphene

Let us introduce Kekule textured graphene as a 2D inversion symmetric higher-order topological insulator. The Hamiltonian for graphene with a Kekule texture is given by

$$H = \sum_{\mathbf{r}\in\Lambda_A} \sum_{j=1}^{3} \left(t + \delta t_j(\mathbf{r})\right) c_A^{\dagger}(\mathbf{r}) c_B(\mathbf{r}+\mathbf{d}_j) + h.c., \tag{2.4}$$

where $c_{A,B}(\mathbf{r})$ indicates the (spinless) electron annihilation operator on the sublattice A, B at the position $\mathbf{r}$, $\mathbf{d}_{1,2,3}$ denotes the vectors connecting an A sublattice site to its neighboring B sublattice sites, and Λ_A denotes the set of the sites belonging to the A sublattice. t denotes the hopping amplitude between nearest neighbor sites, and δt describes the modulation of the hopping amplitudes. When $\delta t = 0$, the Hamiltonian describes the low-energy band structure of graphene having two Dirac points at the Brillouin zone corners with the momentum $\mathbf{k} = \pm\mathbf{K}_+$, while $\delta t_j(\mathbf{r}) = \Delta e^{i\mathbf{K}_+\cdot\mathbf{d}_j} e^{i\mathbf{G}\cdot\mathbf{r}} + \text{c.c}$ couples the two Dirac fermions at the opposite valleys, where $\mathbf{G} = 2\mathbf{K}_+$ [16]. The

unit-cell becomes three times larger than that of pristine graphene, and a Kekule texture is formed. Linearizing H near the Fermi energy, the low-energy Hamiltonian $\int d\mathbf{r}\psi^\dagger(\mathbf{r})H(\mathbf{r})\psi(\mathbf{r})$ becomes

$$H(\mathbf{r}) = -i\sigma_x\tau_z\partial_x - i\sigma_y\tau_z\partial_y + \Delta\tau_x, \tag{2.5}$$

where $\sigma_{x,y,z}$ ($\tau_{x,y,z}$) denote Pauli matrices describing the sublattice (valley) degrees of freedom, and $\psi(\mathbf{r})$ is a four-component spinor. The system is invariant under inversion P, the six-fold rotation about the z-axis C_{6z}, two mirrors M_x and M_y [$M_x : (x, y) \to (-x, y)$, $M_y : (x, y) \to (x, -y)$], and time reversal T symmetries. Thus the system is P symmetric.

Interestingly, we find that the Kekule textured graphene with $\Delta > 0$ ($\Delta < 0$) is a 2D inversion symmetric higher-order topological insulator (HOTI) [6] (a trivial insulator) with $\omega_2 = 1$ ($\omega_{2D} = 0$). A 2D inversion symmetric HOTI with chiral symmetry has a pair of zero-energy corner states related by P symmetry. Moreover, in the presence of an additional mirror symmetry commuting with chiral symmetry, the corner charges are located at mirror invariant corners, manifesting the second-order band topology [10]. Since the Kekule textured graphene has chiral symmetry and M_x mirror commuting with chiral symmetry, there are corner charges localized at the M_x-invariant points when $\Delta > 0$, whereas there is no charge accumulation when $\Delta < 0$; see Fig. 2.1(e), (f). Topology of the Kekule textured graphene is also confirmed by the Wilson loop spectra shown in Fig. 2.1(c), (d). The invariant w_2 is nontrivial when there is a crossing at TRIM point and vice versa. Also, $(-1)^{\omega_2}$ is equivalent to the determinant of the nested Wilson loop, as described in Appendix.

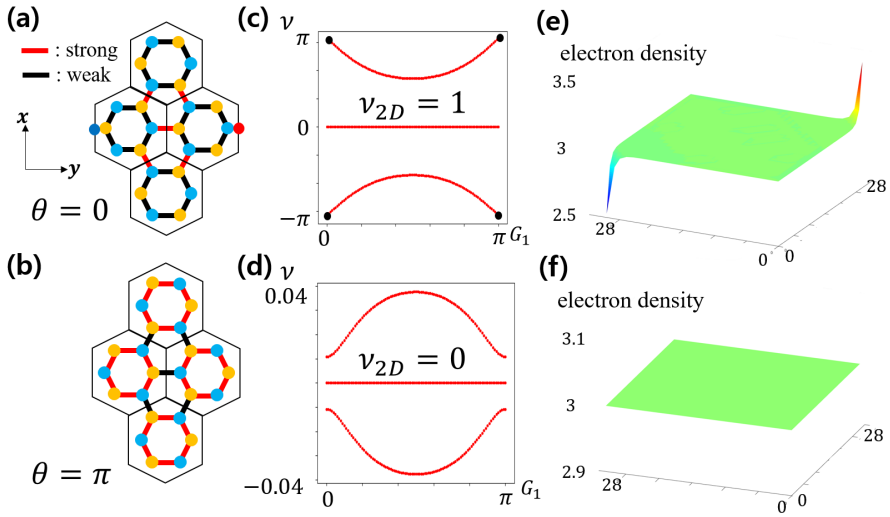

Figure 2.1 (Color online) (a),(b) Finite-size structure of textured graphene. When $\theta = 0$, the intercell hopping is bigger than the intracell hopping, and vice versa when $\theta = \pi$. (c),(d) Wilson loop spectra for $\theta = 0$ and π. The linear crossing point on the $\nu = \pi$ line in (c) shows $\nu_{2D} = 1$. (e),(f) Charge distribution in a finite-size Kekule textured graphene with 28×28 unit cells. Localized states appear at M_x invariant corners when $\nu_{2D} = 1$ whereas the electron density is uniform when $\nu_{2D} = 0$.

2.3 Monolayer graphdiyne

MGD is an experimentally realized planar carbon system composed of sp^2-sp carbon network of benzene rings connected by ethynyl chains [17, 18]. Fig. 2.2(a) describes the unit cell of MGD composed of 18 carbon atoms. Since spin-orbit coupling (SOC) is negligible, MGD can be regarded as a spinless fermion system. The lattice has the same symmetries as the Kekule textured lattice: inversion P, time-reversal T, a two-fold rotation about the x-axis C_{2x}, a six-fold rotation about the z-axis C_{6z}, and a mirror $M_z : z \to -z$ symmetries.

Also, due to the bipartite lattice structure, MGD has chiral (or sublattice) symmetry when only the nearest neighbor hopping between different sublattices is considered, similar to the case of graphene.

Fig. 2.2(b) shows the band structure along with high symmetry directions obtained by first-principles calculations. Here the blue color indicates the bands derived from p_z orbitals while the red color denotes the bands derived from s, p_x, p_y orbitals. Since p_z orbitals are odd whereas s, p_x, p_y orbitals are even under M_z symmetry, the energy spectrum from p_z orbitals is not hybridized with that from s, p_x, p_y orbitals. One can see that the low-energy band structure has approximate chiral symmetry and can be effectively described by using only p_z orbitals. However, to capture the higher-order band topology, the core electronic states derived from s, p_x, p_y orbitals should be included as shown below.

Using the band structure from first-principles calculations and the corresponding parity eigenvalues at TRIMs, one can easily show that MGD is a second-order topological insulator with $w_{1x} = w_{1y} = 0$ and $w_2 = 1$. One interesting feature of the MGD band structure is that we get $w_2 = 0$ when only the bands derived from p_z orbitals are considered. Namely, although the low-energy band structure itself can be well-described by using only p_z orbitals, the higher-order topology can be correctly captured only when the core electronic states derived from s, p_x, p_y orbitals are included. This result can be confirmed by tight-binding analysis as well as first-principles calculations. Since the bands derived from p_z orbitals do not hybridize with those derived from other orbitals because of M_z symmetry, one can compute the relevant topological invariants separately.

The orbital dependence of w_2 can also be confirmed by Wilson loop calculations [6, 10, 19, 20]. Starting from the momentum $\mathbf{k} = (k_1, k_2)$, the set

of Wilson loop eigenvalues $\{e^{i\nu_i(k_2)}\}$, computed along the k_1 direction parallel to the reciprocal lattice vector $\mathbf{G_1}$, indicates the position of Wannier centers at given k_2, and the corresponding charge polarization is given by $p_1(k_2) = \frac{1}{2\pi}\sum_i \nu_i(k_2)$ [21]. The Wilson loop spectrum of MGD shows that the charge polarization is zero in both k_1 and k_2 directions, which is consistent with the parity eigenvalue analysis. Also, the single linear-crossing at $(k_y, \nu) = (0, \pi)$ shown in Fig. 2.2(c) indicates $w_2 = 1$ [6]. Projecting the Wilson loop operator into the p_z (s, p_x, and p_y) orbital basis, we observe $w_2 = 0$ ($w_2 = 1$), which confirms that the higher-order band topology originates from the core electronic levels. The orbital dependence of w_2 can be further confirmed by computing the Wannier center of each orbital explicitly as shown in [21], and also by computing the nested Wilson loop that measures the higher-order band topology [22, 23].

2.3.1 Corner Charges and Filling anomaly

The higher-order band topology of MGD with $w_2 = 1$ induces a pair of anomalous corner states [22]. To see this, we consider a finite-size structure invariant under P symmetry. Tight-binding model analysis shows that when the system is chiral symmetric, there are two robust zero-energy in-gap states related by P whose locations are fixed at M_y-invariant corners [21]. Due to the degeneracy of the two in-gap states, the half-filling condition cannot be satisfied as long as P is preserved, which is known as the filling anomaly [24]. When chiral symmetry is broken, the two degenerate in-gap states can be shifted from zero energy and even merged to the valence (conduction) bands generating a single hole (electron) at half-filling. Namely, the presence of an odd number of holes (electrons) in the valence (conduction) band is the manifestation of the higher-order band topology of generic 2D HOTIs lacking chiral symmetry [11].

To resolve the filling anomaly while keeping P, one needs to add an extra electron (or hole), which leads to the accumulation or depletion of a half-integral charge at each M_y-invariant corner.

Explicitly, let us illustrate how the number of states can be counted in a finite-size HOTI with $w_2 = 1$ following Ref. [11]. When the total number of states is N and chiral symmetry exists, there are $N/2 - 1$ occupied and unoccupied states, respectively, since two in-gap states appear at zero-energy. When chiral symmetry is broken while inversion is preserved, the two in-gap states related by inversion are absorbed into either the valence or the conduction bands simultaneously. Then the number of states below the gap is $n_{\text{gap}} = N/2 \pm 1$. Therefore $n_{\text{gap}} = (\frac{N}{2} + \text{an odd integer})$ when $w_2 = 1$, whereas $n_{\text{gap}} = (\frac{N}{2} + \text{an even integer})$ when $w_2 = 0$. When the valence (conduction) band is completely occupied (unoccupied) by adding electrons or holes additionally, a half-integral electric charge should be accumulated (or depleted) at two corners related by inversion.

For the finite-size MGD composed of $n \times n$ unit cells shown in Fig. 2.3(a), the total number of states are $N = 72n^2$ when $2s$, $2p_x$, $2p_y$, and $2p_z$ orbitals are considered. In MGD, there is a single sp electron localized at every edge of a hexagonal unit cell. If an edge of a unit cell is not shared with an adjacent unit cell, the relevant sp orbital becomes a half-filled zero-energy non-bonding state when chiral symmetry exists. When we consider the geometry of a finite-size structure shown in Fig. 2.3(a), MGD has $8n - 2$ non-bonding states along the boundary. When chiral symmetry is broken, $8n - 2$ states can be merged into the valence band, so that $n_{\text{gap}} = 36n^2 + 4n - 1 = \frac{N}{2} + 4n - 1$. This is what is observed in first-principles calculations and the corresponding density of states is shown in Fig. 2.4. Thus, when all the states below the gap are occupied, and thus the filling anomaly is lifted, a half-integral charge (modulo

an integer charge) is accumulated at two M_y-invariant corners. This can be easily understood because an odd number of non-bonding states exists only at the M_y-invariant corners. [See Fig. 2.3(a).]

To observe the corner states more clearly, we add a hydrogen atom to the carbon atom at every corner, except at two M_y-invariant corners, and keep P and M_y symmetries. Then the number of added hydrogen atoms is an integer multiple of four, which does not alter the band topology of MGD. On the other hand, if two hydrogen atoms are added at the M_y-invariant corners, the total number of bands becomes $N' = N + 2$, while n_{gap} remains the same as described in Fig. 2.4(a). Then $n_{\text{gap}} = \frac{N'}{2} + 4n - 2$ and w_2 becomes trivial. Therefore, the number of added hydrogen atoms should be an integer multiple of four to keep w_2 unchanged. Maximally, $(8n - 4)$ hydrogen atoms can be added to the finite-size MGD with two non-bonding states remaining at M_y-invariant corners. The corresponding density of states is shown in Fig. 2.4(c). Here a half electric charge is accumulated at each M_y-invariant corner when the states below the gap are fully occupied as shown in Fig. 2.4(b).

Since MGD has $w_2 = 1$, when layers of MGD are stacked vertically, the resulting 3D insulator with PT symmetry becomes a 3D weak Stiefel-Whitney insulator when the inter-layer coupling is weak [6]. When inter-layer coupling becomes large enough, an accidental band crossing can happen at a TRIM at which a pair of nodal lines with Z_2 monopole charge is created. The existence of two nodal lines at $k_z = \pm k_c$ ($k_c > 0$) was predicted in ABC-stacked graphdiyne [25], and their Z_2 monopole charge was also confirmed [6] based on first-principles calculations. In ABC-stacked graphdiyne, the 2D subspace with a fixed k_z carries $w_2 = 1$ ($w_2 = 0$) when $|k_z| < k_c$ ($k_c < |k_z| < \pi$) since the band inversion is happened at $\mathbf{k} = (0, 0, \pi)$. Since a 2D HOTI with $w_2 = 1$ possesses corner charges, similar corner charges are also expected in

ABC-stacked graphdiyne in the subspace with a fixed k_z where $w_2 = 1$ [22], which leads to hinge modes of the 3D structure shown in Fig. 2.5(a).

To demonstrate the hinge modes of ABC-stacked graphdiyne, we study a tight-binding model by using only p_z orbitals to reduce numerical costs [21]. The energy spectrum of a finite-size system with PT and C_{2x} symmetries is shown in Fig. 2.5(b), which clearly shows the presence of hinge modes in the momentum region where $w_2 = 1$ as expected. When only p_z orbitals are included, although the low-energy band structure from the tight-binding model is consistent with that from first-principles calculations, the topological property is different. Namely, the tight-binding model predicts $w_2 = 0$ ($w_2 = 1$) when $|k_z| < k_c$ ($k_c < |k_z| < \pi$), which is opposite to the result from the first-principles calculations. Such a discrepancy can be remedied when the core electronic levels are included in the tight-binding calculation, which is confirmed by separate calculations. We believe that our theoretical study provides a way to extend the scope of HOTIs materials to a wider class.

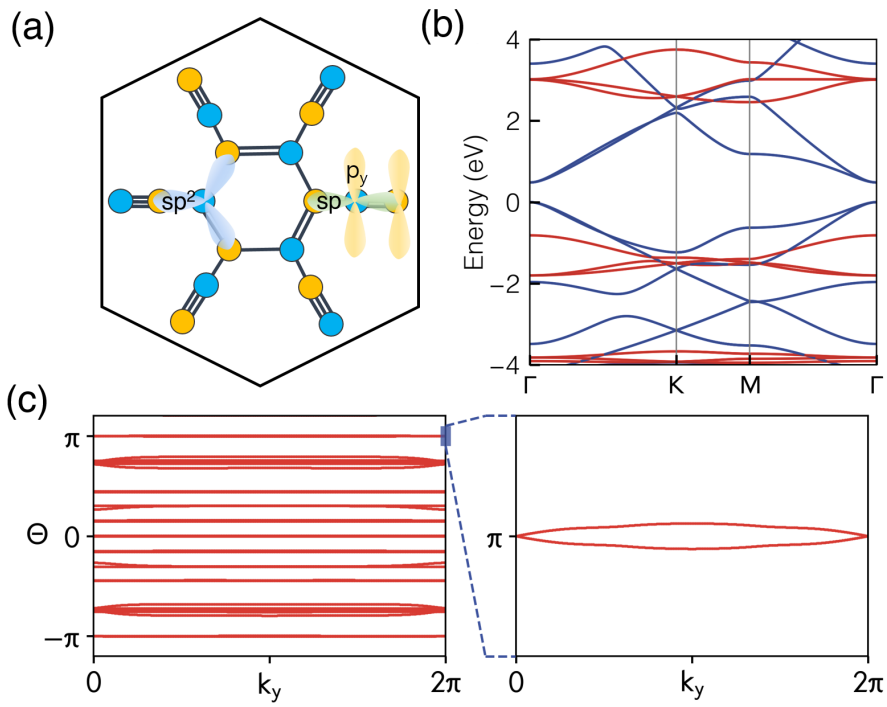

Figure 2.2 (Color online) Lattice structure, band structure, and the Wilson loop spectrum. (a) A schematic figure describing the unit cell and the relevant atomic orbitals of a monolayer graphdiyne (MGD) composed of 18 carbon atoms. Two sublattices are marked with yellow and blue colors, respectively. Since MGD has a bipartite lattice structure, chiral symmetry exists when only the nearest neighbor hoppings are considered. (b) The band structure of MGD obtained by first-principles calculations, which shows approximate chiral symmetry near the Fermi level. Since p_z orbitals are odd while s, p_x, p_y orbitals are even under the mirror $M_z : z \to -z$ operation, the energy spectrum from p_z orbitals (blue) is not hybridized with that from s, p_x, p_y orbitals (red). (c) The Wilson loop spectrum computed including s, p_x, p_y, p_z orbitals. The spectrum exhibits a crossing point at $k_y = 0$, $\theta = \pi$, which indicates $w_2 = 1$.

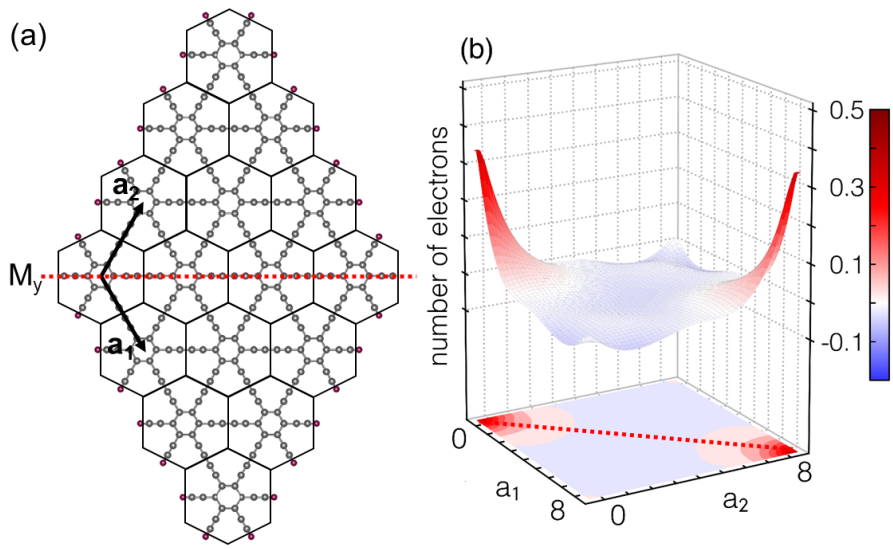

Figure 2.3 (Color Online) Geometry of a finite-size structure and corner charges. (a) A finite-size structure of MGD preserving P and M_y symmetries designed to observe the higher-order band topology protected by P symmetry. The red horizontal line indicates the M_y-invariant line. (b) Electron density distribution for a finite-size MGD composed of 9×9 unit cells where hydrogen atoms are attached at every corner except at the two M_y-invariant corners. To resolve the filling anomaly, we add one electron to MGD additionally and fill the valence band completely. The accumulated or depleted charges with respect to the half-filled configuration are plotted. Here a half-integral charge accumulated at each M_y-invariant corner appears due to the nontrivial 2D topological invariant $w_2 = 1$.

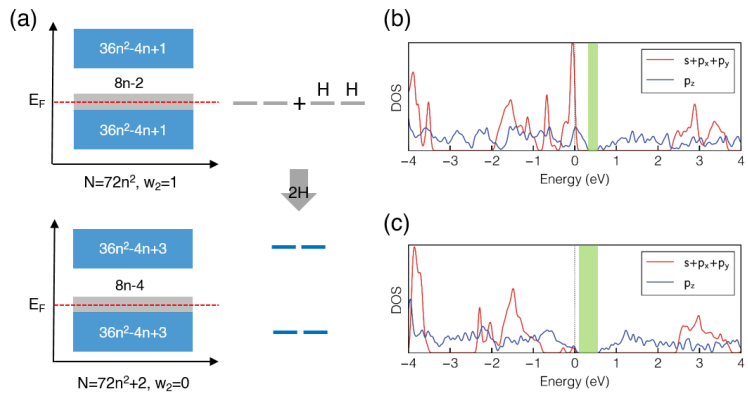

Figure 2.4 (Color Online) Filling anomaly and density of states. (a) A schematic figure displaying the energy spectrum of a finite-size MGD composed of $n \times n$ unit cells, where the total number of states is $N = 72n^2$. Here a thick gray strip near the Fermi level E_F indicates the non-bonding states arising from carbon atoms along the boundary. The upper panel corresponds to the case at half-filling where an odd number of holes is below the gap, which demonstrates the higher-order band topology with $w_2 = 1$. The lower panel shows the case when two hydrogen atoms are added to the finite-size MGD. Here the total number of states N' increases by two ($N' = N + 2$). The hybridization between two hydrogen states and two non-bonding states generates two bonding and two anti-bonding states, so that the number of states below the gap changes from $\frac{N}{2} + 4n - 1$ to $\frac{N'}{2} + 4n - 2$. Then, w_2 also changes from 1 to 0. Thus, to maintain the value of w_2, the number of hydrogen atoms attached for passivation should be an integer multiple of four. (b) Density of states (DOS) of a finite-size MGD without hydrogen passivation. Here the carbon atom at each corner has a non-bonding state. There are $(4n - 1)$ holes below the gap at half-filling. The green color indicate the gapped region. (c) DOS of a finite-size MGD with hydrogen passivation where $(8n - 4)$ hydrogen atoms are attached along the boundary. Here only two carbon atoms at M_y-invariant corners have non-bonding states. There is a single hole below the gap at half-filling. Since both systems in (b) and (c) have an odd number of holes, both are HOTIs with $w_2 = 1$. 21

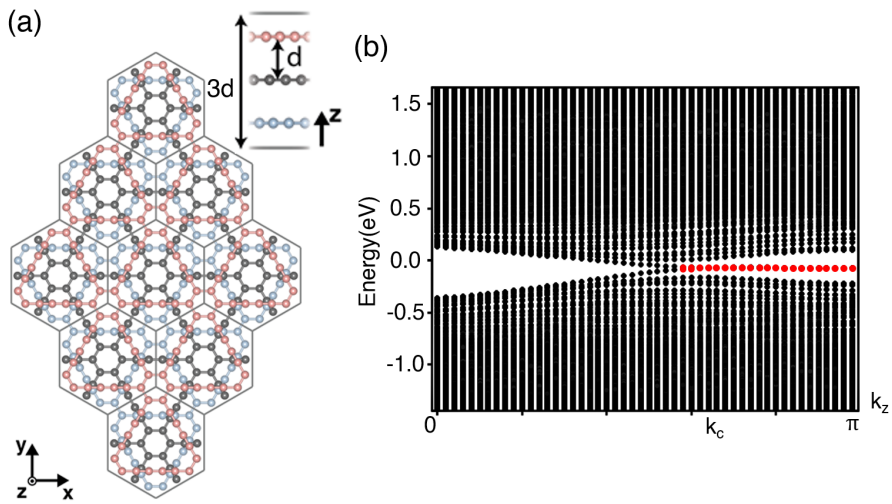

Figure 2.5 (Color Online) Hinge modes of ABC-stacked graphdiyne with monopole nodal lines. (a) A schematic figure describing the 3D geometry of ABC-stacked graphdiyne which is finite in the xy plane but periodic in the vertical direction. The structure must preserve C_{2x} symmetry to carry hinge states. (b) Hinge modes, located in the region $k_c < |k_z| < \pi$, obtained by tight-binding Hamiltonian using only p_z orbitals. In real materials including all core electronic levels, the hinge modes should appear in the region $0 < |k_z| < k_c$ where $w_2 = 1$.

Chapter 3

Fractional charge bound to a vortex in 2D HOTI

Fractional charge localized at topological defects is closely related to the band topology of Bloch wave functions [1, 26–31]. For instance, the one-dimensional (1D) model proposed by Su, Schrieffer, and Heeger (SSH) is a representative system where a half electric charge is localized at a domain wall [1]. The inherent relationship between the zero-mode solution and the topology of Bloch wave functions can be seen from the quantized charge polarization P_1 of the two degenerate ground states, given by $P_1 = 0$ and $P_1 = 1/2$, respectively. The fractional charge accumulated at the domain wall can be determined by the difference of the bulk charge polarization between the two ground states with the distinct quantized charge polarization.

A remarkable idea realizing fractional charge in two-dimensions (2D) is proposed by Hou, Chamon, and Mudry (HCM) in Ref. [16]. Starting from a graphene-like system, whose low-energy excitations are described by massless

Dirac fermions, they showed that a vortex in an order parameter for the Kekule mass gap accommodates a single zero-mode solution manifesting the electron fractionalization in two dimensions. Spontaneous formation of the so-called Kekule texture in graphene leads to the degenerate ground states with broken lattice symmetries [16, 32–34]. Considering the intrinsic relationship between the charge fractionalization and the band topology of the degenerate ground states in the SSH model, the idea of charge fractionalization in 2D systems proposed in the HCM model naturally leads to the following question: what is the fundamental relationship between the zero-mode solution and the bulk band topology of the Bloch wave functions of the degenerate ground states?

In this chapter, we show that the ground state of graphene with a Kekule texture is characterized by a Z_2 topological invariant w_2, which is quantized in 2D systems with P symmetric systems [6, 9]. Two insulating ground states with distinct quantized w_2 values can be interchanged by switching the strong and weak bonds in the Kekule texture, which is similar to the case of the SSH model where two gapped phases with distinct P_1 can be interchanged in an analogous way. Similar to the case of the SSH model, the charge accumulation at a vortex in the order parameter in the HCM model can be obtained from the change in the bulk topological quantity w_2 between the two degenerate ground states with $w_2 = 0$ and $w_2 = 1$, respectively. Furthermore, the change in the bulk topological invariant w_2 around a vortex is described by the quantized magnetoelectric polarizability P_3, which guarantees the presence of a robust mid-gap state confined at the vortex core. We note that the correspondence between the bulk band topology and the vortex bound state in Kekule-textured graphene is beyond the ten-fold classification scheme of defect states proposed by Teo and Kane [31], in which crystalline symmetries are not considered and therefore robust vortex bound states are predicted only

in the presence of chiral or particle-hole symmetry. Since chiral and particle-hole symmetry exists in Kekule-textured graphene, the energy of the mid-gap state is fixed at the Fermi level so that the half-integral value of the accumulated charge at the vortex core is guaranteed. However, even without the chiral symmetry, a quantized fractional charge is localized at the vortex due to the nontrivial bulk band topology of the textured graphene, which is explicitly shown by symmetric Wannier function description. Finally, considering that the magnetoelectric polarizability P_3 is quantized in the presence of the symmetry reversing the space-time orientation, we classify all possible topological crystalline insulators where an order parameter vortex can support fractional charge localized around the vortex core.

3.1 Higher-order band topology of Kekule textured graphene

As we have shown earlier, the Hamiltonian for graphene with a Kekule texture describes HOTI.

$$H = \sum_{\mathbf{r}\in\Lambda_A} \sum_{j=1}^{3} \left(t + \delta t_j(\mathbf{r})\right) c_A^\dagger(\mathbf{r}) c_B(\mathbf{r}+\mathbf{d}_j) + h.c., \tag{3.1}$$

where $\delta t_j(\mathbf{r}) = \Delta(\mathbf{r}) e^{i\mathbf{K}_+\cdot\mathbf{d}_j} e^{i\mathbf{G}\cdot\mathbf{r}} + \text{c.c}$ couples the two Dirac fermions at the opposite valleys, where $\mathbf{G} = 2\mathbf{K}_+$ [16]. A vortex structure of $\Delta(\mathbf{r})$ with the winding number n can be introduced by taking $\Delta(\mathbf{r}) = \Delta_0(\mathbf{r}) e^{in\theta(\mathbf{r})} = \Delta_x(\mathbf{r}) + i\Delta_y(\mathbf{r})$, where $\Delta_{x,y}(\mathbf{r})$ are real functions of $\mathbf{r}$, and the polar angle $\theta(\mathbf{r})$ varies from 0 to 2π encircling the vortex core. Linearizing H near the Fermi energy, the low-energy Hamiltonian $\int d\mathbf{r}\psi^\dagger(\mathbf{r}) H(\mathbf{r}) \psi(\mathbf{r})$ becomes

$$H(\mathbf{r}) = -i\sigma_x\tau_z\partial_x - i\sigma_y\tau_z\partial_y + \Delta_x\tau_x - \Delta_y\tau_y, \tag{3.2}$$

where $\sigma_{x,y,z}$ ($\tau_{x,y,z}$) denote Pauli matrices describing the sublattice (valley) degrees of freedom, and $\psi(\mathbf{r})$ is a four-component spinor. In particular, when $n = 1$, one zero-mode wave function $\psi \sim e^{-\int_0^r dr' \Delta_0(r')}$ is found, yielding a half integral charge $e/2$ localized at the vortex core [16].

3.2 Spectral flow and topological term

Let us explain how the existence of the zero-mode solution is tied to the band topology of the bulk insulator with a uniform Kekule order parameter without vortices. To this end, we define a parameterized Hamiltonian $H(k_x, k_y; \theta)$ describing graphene with a uniform Kekule texture $\Delta(\mathbf{r}) = \Delta_0 e^{i\theta}$, where Δ_0 and θ are constant, and momentum $\mathbf{k} = (k_x, k_y)$. As shown in Fig. 2.1, we use the convention that the inter-unitcell hopping is larger (smaller) than the intra-unitcell hopping when $\theta = 0$ ($\theta = \pi$). When $\theta = 0$ or π, the system is invariant under inversion P, the six-fold rotation about the z-axis C_{6z}, two mirrors M_x and M_y [$M_x : (x, y) \to (-x, y)$, $M_y : (x, y) \to (x, -y)$], and time reversal T symmetries. Thus the system is P symmetric,

The Kekule textured graphene with $\theta = 0$ ($\theta = \pi$) is a 2D inversion symmetric higher-order topological insulator (HOTI) [6] (a trivial insulator) with $w_2 = 1$ ($w_2 = 0$). The fractional charge bound to a vortex can be understood in terms of the charge pumping process during the adiabatic variation of θ around the vortex. The corresponding spectral flow of the energy eigenvalues of $H(k_x, k_y; \theta)$ is plotted in Fig. 3.1. The energy spectrum at each θ is obtained under the open boundary condition that respects inversion symmetry. One can see that one eigenstate travels from the valence (conduction) bands to the conduction (valence) bands during the variation of θ from $-\pi$ to π. The topological origin of such a nontrivial spectral flow can be described as

follows. Under P, the parameterized Hamiltonian $H(k_x, k_y; \theta)$ transforms as

$$PH(k_x, k_y; \theta)P^{-1} = H(-k_x, -k_y; -\theta). \tag{3.3}$$

Thus, when θ is taken as a third momentum k_z, the parameterized Hamiltonian $H_{3\mathrm{D}}(\mathbf{k}) \equiv H(k_x, k_y; \theta = k_z)$ can be considered as a Hamiltonian for a P invariant three-dimensional (3D) insulator. Let us note that, for $H_{3\mathrm{D}}(\mathbf{k})$, the 2D momentum subspaces with $k_z = 0$ and π, respectively, are the only P invariant planes, just like the 2D Hamiltonian $H(k_x, k_y; \theta)$ with $\theta = 0$ and $\theta = \pi$ are the only P invariant models with a Kekule texture. For a 3D insulator with P symmetry, it was recently shown [9, 11] that the quantized magnetoelectric polarizability P_3 is equivalent to $\Delta w_2 = w_2(k_z = \pi) - w_2(k_z = 0)$,

$$\Delta w_2 = 2P_3 = \frac{1}{4\pi^2} \int_{T^2 \times S^1} \mathrm{Tr}\left[AdA - \frac{2i}{3} A^3 \right] \mod 2, \tag{3.4}$$

where $A_{ij} = i\langle u_i | du_j \rangle$ is the non-Abelian Berry's connection characterizing the valence band eigenstates $|u_i\rangle$, T^2 indicates the 2D Brillouin zone, S^1 denotes the unit circle parameterized by θ. Therefore, when $\Delta w_2 = 1 \pmod 2$, the parameterized Hamiltonian $H(k_x, k_y; \theta)$ exhibits quantized magnetoelectric polarizability $P_3 = 1/2$, and one electron should be pumped from the valence bands to the conduction bands and vice versa during the cyclic variation of $\theta \in [-\pi, \pi]$, which corresponds to two chiral hinge modes (the red and blue lines in Fig. 3.1(b)) of the axion insulator described by $H_{3\mathrm{D}}(\mathbf{k})$. Each of these chiral hinge modes is localized at a vortex leading to a pair of vortices carrying a fractional charge as shown in Fig. 3.1(d). This topological charge pumping process underlies the fundamental relationship between the zero-mode solution and the bulk band topology of graphene with a Kekule texture.

3.3 Generalization.

A similar mechanism for charge accumulation at a vortex in a textured lattice due to the topological spectral flow can be applied to any parameterized 2D Hamiltonian $H(k_x, k_y; \theta)$ when its corresponding 3D Hamiltonian $H_{3\mathrm{D}}(\mathbf{k})$ exhibits quantized magnetoelectric polarizability P_3. Namely, $H_{3\mathrm{D}}(\mathbf{k})$ should be the Hamiltonian of an axion insulator. In the following discussions, spin-orbit coupling is not crucial unless noted otherwise. Let us note that P_3 is quantized when the 3D insulator described by $H_{3\mathrm{D}}(\mathbf{k})$ has a space-time orientation reversing symmetry such as $\mathcal{T}$, $\mathcal{P}$, $\mathcal{C}_n\mathcal{T}$, and $\mathcal{C}_n\mathcal{P}$ ($n = 2, 3, 4, 6$) [4,9,35,36], where we have used caligraphic fonts for symmetries in the 3D space to distinguish them from the symmetries in the 2D space denoted in italic fonts. Among these symmetries, we can neglect $\mathcal{C}_{3z}\mathcal{T}$ in that a $\mathcal{C}_{3z}\mathcal{T}$-symmetric axion insulator is expected to carry the same topological properties as the one with $\mathcal{T}$ symmetry only, because $(\mathcal{C}_{3z}\mathcal{T})^3 = \mathcal{T}$ and $(\mathcal{C}_{3z}\mathcal{T})^2 = \mathcal{C}_{3z}^{-1}$, and $\mathcal{C}_{3z}$ by itself cannot quantize P_3. Likewise, we do not have to consider $\mathcal{C}_{6z}\mathcal{T}$ since $(\mathcal{C}_{6z}\mathcal{T})^3 = \mathcal{C}_{2z}\mathcal{T}$. For $\mathcal{C}_{nz}\mathcal{P}$ symmetries, $(\mathcal{C}_{3z}\mathcal{P})^3 = \mathcal{P}$ and $(\mathcal{C}_{6z}\mathcal{P})^3 = \mathcal{C}_{2z}\mathcal{P} = \mathcal{M}_z$. Thus, we only have to consider $H_{3\mathrm{D}}(\mathbf{k})$ with $\mathcal{T}$, $\mathcal{P}$, $\mathcal{C}_{2z}\mathcal{P}$, $\mathcal{C}_{2z}\mathcal{T}$, $\mathcal{C}_{4z}\mathcal{P}$, or $\mathcal{C}_{4z}\mathcal{T}$ symmetries. It is worth noting that in each axion insulator phase described by $H_{3\mathrm{D}}(\mathbf{k})$, the 2D subspaces with $k_z = 0$ and $k_z = \pi$, respectively, support distinct 2D topological invariants. Namely, the quantized P_3 of $H_{3\mathrm{D}}(\mathbf{k})$ can be obtained from the difference between the 2D topological invariants on the two symmetry invariant planes with $k_z = 0$ and $k_z = \pi$, respectively. This ensures that the corresponding vortex structure described by $H(k_x, k_y, \theta)$, which connects two distinct topological phases at $\theta = 0$ and π, hosts a bound state with a fractional charge at the vortex core.

Now let us explain how the symmetry of the 3D Hamiltonian $H_{3\mathrm{D}}(\mathbf{k})$ can

3D Symmetry	2D Symmetry	SOC	2D TI
$\mathcal{P}=\mathcal{C}_{2z}\mathcal{M}_z$	C_{2z}, C_{6z}		Atomic
$\mathcal{C}_{4z}\mathcal{P}=(\mathcal{C}_{4z}\mathcal{M}_z)^3$	C_{4z}		Atomic
$\mathcal{T}$	T	O	QSHI
$\mathcal{M}_z$	M_z		Mirror TI
$\mathcal{C}_{2z}\mathcal{T}$	$C_{2z}T$, $C_{6z}T$		SWI (Atomic)
$\mathcal{C}_{4z}\mathcal{T}$	$C_{4z}T$	O	Atomic

Table 3.1 The correspondence between the symmetry of $H_{3\mathrm{D}}(\mathbf{k})$ exhibiting quantized magnetoelectric polarizability P_3 and that of the 2D Hamiltonian $H(k_x,k_y;\theta=0,\pi)$. For T and C_4T symmetry, spin orbit coupling (SOC) is necessary to have $P_3=1/2$. (See Supplemental Materials). The nature of the corresponding 2D topological insulator (TI) is also shown. Here "Atomic" denotes an obstructed atomic insulator, "SWI" means Stiefel Whitney insulator.

be related with that of the physical 2D parametrized Hamiltonian $H(k_x,k_y;\theta)$. For instance, as in the case of graphene with a Kekule texture, if the system with a uniform order parameter is invariant under n-fold rotation C_n about the z axis at $\theta=0$ and π, but not at other θ values, then the C_n symmetry can be implemented as

$$C_nH(k_x,k_y;\theta)C_n^{-1}=H(k_x',k_y';-\theta), \tag{3.5}$$

where k_x', k_y' are the rotated momenta after C_n operation. Due to the sign change of θ under C_n, the 2D system is C_n invariant only at $\theta=0,\ \pi$. Then the C_n symmetry of the 2D system can be implemented in $H_{3\mathrm{D}}(\mathbf{k})$ as the $\mathcal{C}_n\mathcal{M}_z$ symmetry. Then we ask whether $\mathcal{C}_n\mathcal{M}_z$ symmetry can quantize P_3 and also whether C_n symmetry supports a 2D topological invariant ν_{2D} such that its difference $\Delta\nu_{2D}=\nu_{2D}(\theta=\pi)-\nu_{2D}(\theta=0)$ is identical to $2P_3$ (modulo

two).

First, if $H(k_x, k_y; \theta = 0, \pi)$ is C_{2z}(or P) invariant as the Kekule textured graphene, the relevant 3D Hamiltonian $H_{\rm 3D}(\mathbf{k})$ describes an inversion symmetric ($\mathcal{P} = \mathcal{C}_{2z}\mathcal{M}_z$) axion insulator. Similarly, if $H(k_x, k_y; \theta = 0, \pi)$ is C_{6z} invariant, $H_{\rm 3D}(\mathbf{k})$ can have quantized P_3, since $\mathcal{P} = (\mathcal{C}_{6z}\mathcal{M}_z)^3$. In the case of C_{4z} symmetry, the corresponding 3D system has $\mathcal{C}_{4z}\mathcal{P}$ symmetry as well, which is another symmetry quantizing P_3. Moreover, since $C_{2z,4z,6z}$ symmetry can support a 2D invariant ν_{2D} satisfying $\Delta\nu_{2D} = 2P_3$ [11, 37], the parameterized Hamiltonian $H(k_x, k_y; \theta)$ can support a bound state at the vortex. For C_{3z} symmetry, however, applying C_{3z} three times to Eq. (3.5) yields $H(k_x, k_y; \theta) = H(k_x, k_y; -\theta)$, which is not adequate to describe a vortex structure.

If $H(k_x, k_y; \theta = 0, \pi)$ is invariant under $S = M_z$, T, or C_nT, the S symmetry can be implemented as

$$SH(k_x, k_y; \theta)S^{-1} = H(k'_x, k'_y; -\theta), \tag{3.6}$$

where the relevant 3D Hamiltonian is also symmetric under $\mathcal{S} = \mathcal{M}_z$, $\mathcal{T}$, $\mathcal{C}_n\mathcal{T}$. Let us note that M_z, T, $C_{2z}T$, $C_{4z}T$, $C_{6z}T$ symmetries support a 2D invariant ν_{2D} satisfying $\Delta\nu_{2D} = 2P_3$, whereas $C_{3z}T$ can support only a quantum spin Hall insulator (QSHI) in the presence of spin orbit coupling due to $(C_{3z}T)^3 = T$.

Table I summarizes the correspondence between the symmetry of the 2D insulator with a uniform gap-opening order parameter, described by the Hamiltonian $H(k_x, k_y; \theta = 0, \pi)$, and the symmetry of the relevant 3D Hamiltonian $H_{\rm 3D}(\mathbf{k})$ exhibiting quantized P_3. When the two Hamiltonian $H(k_x, k_y; \theta = 0)$ and $H(k_x, k_y; \theta = \pi)$ support distinct bulk topological properties, a fractional charge can be localized at the core of a vortex in the order parameter parame-

terized by θ due to the topological spectral flow associated with the quantized P_3. Let us note that in the case of the Kekule textured graphene, which has C_{2z} symmetry for $\theta = 0$, π and T symmetry for any θ, the quantization of P_3 of the relevant 3D Hamiltonian is guaranteed by either $\mathcal{P}$ or $\mathcal{C}_{2z}\mathcal{T}$.

In the case of the other symmetries C_{2z}, C_{4z}, $C_{2z}T$, $C_{4z}T$ which are nonlocal in 2D real space, the insulators described by $H_D(\theta = 0, \pi)$ can have higher-order band topology. The minimal Dirac Hamiltonian $H_D(\theta = 0, \pi)$ can be considered as two copies of Chern insulators with opposite Chern numbers. After suitable regularization, either one of $H_D(\theta = 0)$ or $H_D(\theta = \pi)$ supports a pair of counter propagating chiral edge modes whereas the other has no edge state. For the Hamiltonian with chiral edge modes, one can introduce additional surface mass terms, compatible with the corresponding nonlocal symmetry, that induce domain walls of the surface mass terms [22, 38, 39]. Because of the domain walls, the insulator can support localized corner charges in the presence of additional chiral symmetry exhibiting second-order band topology. The adiabatic variation of θ interpolating a second-order topological insulator and a trivial insulator can also be described by the axionic topological response with $P_3 = 1/2$ [9, 11] as shown in Appendix [21].

In real materials, the U(1) symmetry of the order parameter may be reduced to a discrete $\mathrm{Z}_{n=2,3,4,6}$ symmetry due to lattice potentials. However, fractional charges can still be localized at a vortex with discrete symmetry as long as the phase θ of the order parameter winds 2π around the vortex, as in the case of Kekule textured graphene where three domains with $\theta = 0$, $2\pi/3$, $4\pi/3$, respectively, meet at a junction with localized charges [40]. Bound charges at the junction with $\mathbb{Z}_4$ symmetry proposed in 2D insulators with quantized quadrupole moment [41] can also be explained by our theory. Another interesting way to observe fractional bound charges is to construct

heterostructures composed of 2D topological and normal insulators. For instance, a bound state should be present at a junction where a QSHI and two ferromagnetic insulators with opposite in-plane magnetization meet. Similar heterostructures can be constructed for many 2D topological crystalline insulators as discussed explicitly in Appendix [21].

One interesting direction for future research is to extend the idea of symmetry protected topological vortices to defects of various codimensions. For example, it is shown in Ref. [31] that a point defect carrying fractional charges in 3D systems can be described by using the Hamiltonian for five-dimensional insulators whose topological invariant has the Chern-Simons 5-form. Systematic classification of such defect structures taking into account space group symmetries is desirable to complete the classification table for defect Hamiltonian beyond the tenfold classification scheme proposed before [31].

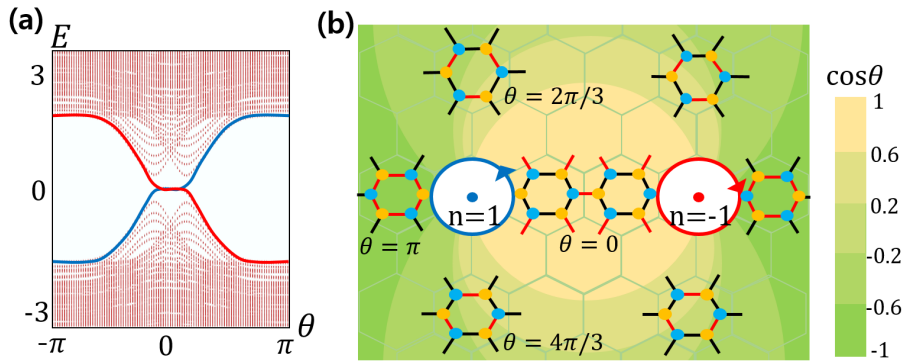

Figure 3.1 (Color online) (a) Schematic figure describing the lattice geometry around a vortex in Kekule textured graphene. Far from the vortex center, Kekule texture varies slowly as θ changes. At $\theta = 0$, the textured graphene is a 2D inversion symmetric HOTI (ν_{2D}=1) whereas it is a trivial insulator (ν_{2D}=0) at $\theta = \pi$. (b) Spectral flow around the vortex as a function of θ. During one cycle, one state travels from the valence (conduction) bands to the conduction (valence) bands crossing the Fermi level. The existence of two chiral modes (the blue and red lines) implies that vortices with the opposite winding numbers must be pair created. (c) The parameterized Hamiltonian $H(k_x, k_y; \theta)$ can be thought of as that for a $3D$ P symmetric axion insulator, where the $k_z = 0$ plane describes a 2D inversion symmetric HOTI, whereas the $k_z = \pi$ plane describes a trivial insulator. Here $+$, $-$ denote the parity of occupied bands at time-reversal invariant momenta. (d) Vortex-antivortex pair created in a uniform background with $\theta = \pi$, arising from the topological spectral flow around the vortices.

Chapter 4

Summary

Quasi-particle excitations carrying fractional charges are one of the most intriguing subjects in the study of correlated quantum matter. An archetypal 1D model Hamiltonian exhibiting charge fractionalization is the SSH model that describes the low-energy band structure of polyacetylene, where two degenerate ground states are formed due to spontaneous dimerization. The charge bound at the domain wall is equivalent to the difference of charge polarization between the two degenerate ground states and therefore takes the value 1/2, as the bulk polarization P is quantized to P=0 or P=1/2 modulo 1 due to inversion symmetry. This example clearly demonstrates the fundamental relationship between the fractionally charged bound states and the symmetry protected band topology.

Fractional excitation also emerges in 2D HOTIs. As a prototypical example, we suggest Kekule textured graphene as a 2D HOTI protected by inversion symmetry. Plus, we theoretically propose monolayer graphdiyne (MGD) as the

first realistic candidate material for a 2D HOTI protected by inversion symmetry. Based on first-principles calculations and tight-binding model analysis, we explicitly demonstrate in a finite-size MGD, the filling anomaly at half-filling and the accumulation of half-integral charges at two corners after adding an electron. Moreover, we further show that the higher-order band topology of MGD is protected by a 2D topological invariant, which explicitly measures the higher-order band topology protected by inversion symmetry. In particular, we explicitly demonstrate that the higher-order band topology of 2D HOTIs can be directly proved via filling anomaly at half-filling and the accumulation of half-integral charges at corners after adding one electron, even if real materials do not possess chiral symmetry. We show that the higher-order band topology of MGD is the fundamental origin of the nontrivial band topology of a related 3D material, ABC-stacked graphdiyne, which can be obtained via ABC-type vertical stacking of MGD.

In chapter 3, we show how the charge fractionalization in 2D Kekule textured graphene is related to its bulk band topology. We show that the Hamiltonian describing a vortex structure can be identified with an effective three-dimensional (3D) Hamiltonian by considering the angular coordinate around a vortex as a third coordinate, and that the resulting three-dimensional effective Hamiltonian exhibits a nonzero quantized magnetoelectric polarization. Namely, the effective 3D Hamiltonian can be considered as a Hamiltonian for a 3D axion insulator, and the spectral flow during the adiabatic pumping process corresponds to its chiral hinge modes, which eventually determines the accumulated charge localized at the vortex core. Furthermore, we generalize this mechanism of charge fractionalization to any 2D insulators carrying a nontrivial topological invariant whose low-energy effective 2D Hamiltonian with an order parameter vortex can be considered as a Hamiltonian for a 3D

axion insulator. Using the fact that the magnetoelectric polarization is quantized in the presence of any symmetry that reverses the space-time orientation, we classify all possible topological crystalline insulators whose order parameter vortex carries a fractional charge at the vortex core. Although there are a couple of previous theoretical studies on charge accumulation at topological defects in 2D systems, only non-spatial local symmetries such as chiral symmetry or particle-hole symmetry have been considered in those studies. Our theory, however, shows that 2D topological crystalline insulators can accommodate charge fractionalization even in the absence of such non-spatial symmetries. This result is a critical step forward to the generalization of the fundamental relationship between a fractional charge bound to a vortex and the band topology protected by crystalline symmetries in 2D and higher dimensions.

Appendix A

Nested Wilson loop

A Wilson loop is a gauge invariant observable whose eigenvalue spectrum contains the information on the topological properties of the Hamiltonian. A Wilson loop operator is defined by

$$\begin{aligned} W_{(k_1+2\pi,k_2)\leftarrow(k_1,k_2)} &\equiv W_{x,\mathbf{k}} \\ &= \lim_{N\to\infty} F_{N-1}F_{N-2}\cdots F_1F_0 \\ &= Pe^{-i\oint_C A_k dk}, \end{aligned} \tag{A.1}$$

where $[F_i]_{nm} = \langle u_m(k_{i+1},k_2)|u_n(k_i,k_2)\rangle, k_i = \frac{2\pi}{N}i$ and $m,n = 1,\cdots,N_{occ}$. Since a Wilson loop operator is unitary, the eigenvalue equation is given by $W_{x,\mathbf{k}}|\nu^j_{x,\mathbf{k}}\rangle = e^{i\nu^j_x(k_y)}|\nu^j_{x,\mathbf{k}}\rangle$, where $\nu^j_x(k_y)$ corresponds to x-component of Wannier center of jth Wannier functions. It follows that the electron charge polarization is expressed as $P_{1,x} = \frac{1}{2\pi N_y}\sum_{k_y}\sum_j \nu^j_x(k_y) = -\frac{i}{2\pi}\log\det[W_{x,\mathbf{k}}] = -\frac{1}{2\pi}\oint \mathrm{Tr}[A_k]dk$. In the presence of P symmetry, the set of eigenvalues satisfy $\{\nu_x(k_y)\} \equiv \{-\nu_x(-k_y)\}$ mod 2π, so that the polarization is quantized into either 0 or 1/2 modulo 1.

Recently, the nested Wilson loop method was developed to study higher-order topological properties [23, 41]. The procedure for computing the nested Wilson loop is as follows. First, we calculate a Wilson loop operator along a reciprocal vector $\mathbf{G_x}$, where its eigenvalues are $\{e^{i\nu_x(k_y)}\}$. Next, we choose a certain subset of Wilson loop eigenvalues $\{\nu_x\}$ and find the corresponding Wannier eigenfunctions$\{|\nu_x(k_y)\rangle\}$. With the eigenfunctions, we calculate a Wilson loop operator along the other reciprocal vector $\mathbf{G_y}$, so we obtain a nested Wilson loop operator $\tilde{W}$ as

$$\tilde{W}_{k_y+2\pi\leftarrow k_y} = \tilde{W}_y = \lim_{N\to\infty} \tilde{F}_{N-1}\tilde{F}_{N-2}\cdots\tilde{F}_1\tilde{F}_0, \tag{A.2}$$

where $[\tilde{F}_i]_{nm} = \langle\nu_m(k_{i+1})|\nu_n(k_i)\rangle, k_i = \frac{2\pi}{N}i$ and $m, n = 1, \cdots, N_{\text{sub}}$. Here N_{sub} denotes the number of the subbands of a gapped Wilson loop spectrum. By using this method, it is possible to detect the electric multipole moments of the system [23, 41, 42].

The Kekule textured graphene has spinless T symmetry. In the presence of PT symmetry, the Wilson loop spectrum satisfies $\{\nu_x\} \equiv \{-\nu_x\} \mod 2\pi$. Thus, $\nu_x(k_y)$ must be $0, \pi$ or exist as a pair $\{+\nu, -\nu\}$, so that the Wilson loop spectrum can be divided into two subsets that are centered at either $\nu = 0$ or $\nu = \pi$. We choose the Wannier sector centered at $\nu = \pi$, and calculate the nested Wilson loop. Due to PT symmetry, $P_{1,y}^{\nu_x} \equiv -P_{1,y}^{-\nu_x} \mod 1$, so that Wannier sector polarization is quantized into $1/2$ or 0 and the determinant of $\tilde{W}$ is either -1 or 1, respectively [23, 41]. It is known that the determinant of the nested Wilson loop is the same as $(-1)^{w_2}$ [10]. For the Kekule textured graphene, PT (or $C_{2z}T$) symmetry exists when $\theta = 0$ or π. In Fig. A.1, the Wilson loop spectrum of Kekule textured graphene is shown, where $\det(\tilde{W})$ is quantized as -1 for $\theta = 0$ while $\det(\tilde{W})$ is quantized as 1 for $\theta = 0$. As θ varies, we observe that the Wilson loop spectrum undergoes a phase transition between $\theta = 0$ and $\theta = \pi$. $\det(\tilde{W})$ changes abruptly, and the gap of the Wilson

spectrum is closed at a critical point.

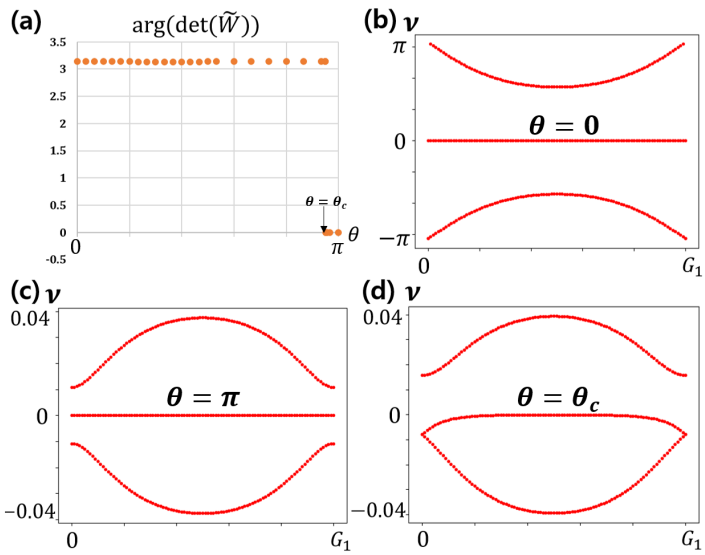

Figure A.1 (Color online) (a) The determinant of nested Wilson loops for the model Hamiltonian describing the Kekule textured graphene, which is plotted for $0 \leq \theta \leq \pi$. At $\theta = \theta_c$, $\det(\tilde{W})$ changes abruptly. (b) The Wilson loop spectrum for $\theta = 0$. The spectrum has a Dirac-like crossing point at $k = 0$, and the determinant of the nested Wilson loop is -1. (c) The Wilson loop spectrum for $\theta = \pi$. The Wilson loop spectrum of a trivial insulator has no band crossing and the determinant of the nested Wilson loop is 1. (d) The Wilson loop spectrum for $\theta = \theta_c$, where the gap is closed, which implies the phase transition between $\det(\tilde{W}) = -1$ and $+1$.

Appendix B

Classification of axion insulators by crystalline symmetries.

In the main text, we mentioned that space-time orientation reversing symmetries quantize magnetoelectric polarizability P_3, and $H_{3\mathrm{D}}(\mathbf{k})$ describes a 3D axion insulator. The corresponding symmetries of $H(k_x, k_y, \theta = 0,\ \pi)$ are P, T, M_z, $C_{2z}T$, $C_{4z}P$ and $C_{4z}T$. The quantized P_3 of each 3D axion insulator can be described by a pumping process of 2D invariants that are defined at two different symmetry invariant planes with $k_z = 0$ and π. Among the symmetries, T and M_z symmetric axion insulators are described by a pumping process of topological phases with the first order band topology (QSHI and mirror Chern insulators) and trivial phases. For the other symmetries, the fractional charge at the order parameter vortex is described by a pumping process of a higher-order topological insulator (HOTI) and a trivial insulator. Here, we explicitly describe the low energy Hamiltonian and its physical property for each symmetry class.

$\mathcal{T}$ symmetry.— 3D time-reversal invariant Z_2 TI is described by a pumping process between a QSHI and a trivial insulator defined at the $k_z = 0$ and π planes [43]. Let us note that SOC is crucial since 2D AI class is trivial according to the tenfold classification [44]. The low energy Hamiltonian for a 2D QSHI is

$$H(\mathbf{k}) = i\partial_x \tau_x \sigma_x + i\partial_y \tau_x \sigma_y + M\tau_z \sigma_0, \tag{B.1}$$

where Pauli matrices τ and σ represent orbital and spin degrees of freedom and time reversal symmetry is $T = \sigma_y K$ satisfying $TH(\mathbf{k})T^{-1} = H(-\mathbf{k})$. The corresponding gapped insulator should be either a QSHI ($M > 0$) or a trivial insulator ($M < 0$) depending on the sign of the mass M [5]. The Hamiltonian with a vortex can be expressed as

$$\begin{aligned} H(k_x, k_y, \theta) = {} & i\partial_x \tau_x \sigma_x + i\partial_y \tau_x \sigma_y \\ & + \Delta \cos\theta \tau_z \sigma_0 + \Delta \sin\theta \tau_x \sigma_z, \end{aligned} \tag{B.2}$$

where $\tau_x \sigma_z$ anticommutes with other matrices and it is odd under time reversal symmetry, so that the vortex structure breaks time-reversal symmetry except at $\theta = 0$ (a trivial insulator) and at $\theta = \pi$ (a QSHI).

As shown in Fig. B.1 (a), a vortex structure can also be realized at the junction where a QSHI ($\theta = \pi$) and two ferromagnetic insulators ($\theta = \pm\alpha$) with in-plane magnetization meet. The Hamiltonian describing the gapless surface of the QSHI is

$$\begin{aligned} H_0 &= v_F \int dx (\psi_R^\dagger i\partial_x \psi_R - \psi_L^\dagger i\partial_x \psi_L), \\ &= v_F \int dx \Psi^\dagger i\sigma_z \partial_x \Psi, \end{aligned} \tag{B.3}$$

where $\psi_{R/L}$ is the right/left moving states and $\Psi^\dagger = (\psi_R^\dagger, \psi_L^\dagger)$. The ferromagnetic insulators introduce time-reversal breaking mass terms that open

the band gap of the edge state. The resulting the surface Hamiltonian is $H = H_0 + m_1\sigma_x + m_2\sigma_y$. Parametrizing $m_1 = m\cos\phi$, $m_2 = m\sin\phi$, the charge density at the magnetic domain is expressed as $\rho = \frac{1}{2\pi}\partial_x\phi$ [28]. When the spin direction is reversed, the sign of the mass terms is also reversed ($\phi \to \phi + \pi$). Thus, the mass gap is closed at the junction, indicating a zero-mode state and fractional charges bound at the vortex center $Q = \int \rho dx = 1/2$ [45].

$\mathcal{M}_z$ symmetry.— For $\mathcal{M}_z$ symmetry, a mirror Chern number C_m can be defined on the $k_z = 0$ and $k_z = \pi$ planes. C_m is given by the difference of the Chern number C of two sectors with different mirror eigenvalues. The difference of the mirror Chern numbers on these planes corresponds to $2P_3$, that is, $C_m(k_z = 0) - C_m(k_z = \pi) \equiv 2P_3 \mod 2$ [9]. Let us consider the low energy Hamiltonian describing a 2D mirror Chern insulator (MCI).

$$H(\mathbf{k}) = i\partial_x\Gamma_1 + i\partial_y\Gamma_2 + M\Gamma_3, \tag{B.4}$$

where $\Gamma_1 = \tau_x\sigma_x$, $\Gamma_2 = \tau_x\sigma_y$, $\Gamma_3 = \tau_z$. The mirror operator $M_z = -i\Gamma_1\Gamma_2\Gamma_3 = \tau_z\sigma_z$ satisfies $M_z H(\mathbf{k}) M_z^{-1} = H(\mathbf{k})$. Considering the projection operator $P_\pm = \frac{1}{2}(1 \pm \tau_z\sigma_z)$, the Hamiltonian can be expressed as a direct product of two Hamiltonians that have opposite mirror eigenvalues: $H = P_+H \oplus P_-H$. Depending on the mass sign, the Hamiltonian describes either a MCI ($M > 0, H = H_{C=+1} \oplus H_{C=-1}$) or a trivial insulator ($M < 0$) [46]. The Hamiltonian with a vortex is given by

$$\begin{aligned} H(\mathbf{k}, \theta) = {} & i\partial_x\tau_x\sigma_x + i\partial_y\tau_x\sigma_y \\ & + \Delta_1\cos\theta\tau_z\sigma_0 + \Delta_2\sin\theta\tau_x\sigma_z, \end{aligned} \tag{B.5}$$

where $\tau_x\sigma_z$ is odd under mirror symmetry, so that the vortex structure breaks mirror symmetry except at $\theta = 0$ and π. Similar to the case with $\mathcal{T}$ symmetry, a vortex structure is realizable at a junction where a MCI and two mirror

symmetry broken insulators meet. As shown in the Fig. B.1 (b), in spin orbit coupled systems, two ferromagnetic insulators with anti-parallel in-plane magnetization break mirror symmetry, introducing surface mass terms with opposite sign, so that fractional charges can be localized at the vortex core. In spinless fermion systems, the ferromagnetic insulators can be replaced by two ferroelectric insulators with anti-parallel out-of-plane charge polarization.

$\mathcal{P}$ symmetry.— Except for the cases with $\mathcal{T}$ and $\mathcal{M}_z$ symmetries, the quantized magnetoelectric polarizability P_3 of the axion insulators associated with other symmetries can be described by the pumping process between a higher-order topological insulator and a trivial insulator. The inversion symmetric axion insulator can be described by the pumping process between a C_{2z} protected higher-order TI and a trivial insulator. The corresponding low energy Dirac Hamiltonian can be written as

$$H(k_x, k_y, \theta) = k_x\Gamma_1 + k_y\Gamma_2 + M\cos\theta\Gamma_3 + M\sin\theta\Gamma_4, \tag{B.6}$$

where we take $C_{2z} = \Gamma_3 = \tau_z$, $\Gamma_1 = \tau_x$, $\Gamma_2 = \tau_y\sigma_z$. One can clearly see that $H(k_x, k_y, \theta)$ is C_{2z} symmetric only at $\theta = 0,\ \pi$. Since the coefficient of the Γ_3 term has the opposite sign at $\theta = 0$ and $\theta = \pi$, the number of the occupied bands with the negative C_{2z} eigenvalue is also different by two. Considering that the Z_2 invariant ν_{2D} of a C_{2z} symmetric 2D insulator is expressed by the product of C_{2z} eigenvalues at time reversal invariant momenta (TRIM) Γ_i as

$$(-1)^{\nu_{2D}} = \prod_{i=1}^{4}(-1)^{[N^-_{\rm occ}(\Gamma_i)/2]}, \tag{B.7}$$

where $N^-_{\rm occ}(\Gamma_i)$ is the number of the occupied states with the negative C_{2z} eigenvalues at the momentum Γ_i. For a 2D higher-order TI, $\nu_{2D} \equiv 1 \mod 2$ and the corresponding topological invariant for the axion insulator is given by $\nu_{2D}(k_z = 0) - \nu_{2D}(k_z = \pi) \equiv 2P_3 \mod 2$ [11]. The second order topology

of the $\nu_{2D} = 1$ phase can be understood as follows. Using the symmetry representation of Γ matrices, the above Dirac Hamiltonian at $\theta = 0,\ \pi$ can be viewed as two copies of Chern insulators with the opposite Chern numbers. After suitable regularization by addition terms quadratic in momentum, one can make $H(\theta = 0)$ to have a pair of counter-propagating edge modes whereas $H(\theta = \pi)$ has no edge mode. Then by adding C_{2z} symmetric mass terms to $H(\theta = 0)$, one can find corner charges at the location where the sign of the surface mass terms changes [47].

$\mathcal{C}_{4z}\mathcal{P}$ symmetry.— The $\mathcal{C}_{4z}\mathcal{P}$ invariant axion insulator can be described by the pumping process between two different C_{4z} invariant insulators defined on the $k_z = 0$ and $k_z = \pi$ planes [37]. For a 2D C_{4z} invariant insulator, the corner charge Q_C is quantized as $Q_C = \frac{N_C}{4} \mod 1$, where N_C denotes the number of electrons whose Wannier center is located at the Wycoff position C. Thus, the higher-order band topology of $2D$ C_{4z} invariant insulators is characterized by a $\mathbb{Z}_4$ invariant. However, a $C_{4z}P$ symmetric axion insulator is characterized by a $\mathbb{Z}_2$ invariant, which detects the difference of the corner charges defined on the $k_z = 0$ and $k_z = \pi$ planes, respectively [37]. The $\mathbb{Z}_2$ nature arises because C_{2z} symmetry exists on every k_z plane so that the set of C_{2z} eigenvalues on the $k_z = 0$ and $k_z = \pi$ planes must be same in an insulating phase. Thus, the change of N_C must be an even integer such as

$$N_C(k_z = \pi) - N_C(k_z = 0) = 0 \text{ or } 2 \mod 4. \tag{B.8}$$

Now let us consider the following low energy Dirac Hamiltonian

$$H(\mathbf{k}, \theta) = k_x\Gamma_1 + k_y\Gamma_2 + M\cos\theta\Gamma_3 + M\sin\theta\Gamma_4, \tag{B.9}$$

where $\Gamma_1 = \sigma_x, \Gamma_2 = \sigma_y, \Gamma_3 = \tau_z\sigma_z, \Gamma_4 = \tau_y\sigma_z, \Gamma_5 = \tau_x\sigma_z$, and $C_{4z} = \text{diag}[1, i, -1, -i] = \tau_z \otimes \begin{pmatrix} 1 & 0 \\ 0 & i \end{pmatrix}$. Then from $C_4\Gamma_1C_4^{-1} = \Gamma_2$ and $C_4\Gamma_2C_4^{-1} = -\Gamma_1$, one can see

the C_{4z} invariance of the Hamiltonian at $\theta = 0,\ \pi$, $C_4 H(\mathbf{k}, \theta = 0,\ \pi) C_4^{-1} = H(C_4\mathbf{k}, \theta = 0,\ \pi)$.

At $\theta = 0,\ \pi$, the wave functions of the occupied states are $[0, 1, 0, 0]^T$ and $[0, 0, 1, 0]^T$ when $M > 0$, with the corresponding C_{4z} eigenvalues, i and -1, respectively. On the other hand, when $M < 0$, the wave functions of the occupied states are $[1, 0, 0, 0]^T$ and $[0, 0, 0, 1]^T$ with the corresponding C_{4z} eigenvalues, 1 and $-i$, respectively. One can clearly see that the C_{2z} eigenvalues of the occupied states remains the same independent of the sign of M. In this case, $\Delta N_C = 2 \mod 4$ as shown in Ref. [37], and the sign reversal of M describes the nontrivial $\mathbb{Z}_2$ invariant of the axion insulator.

On the other hand, when $\theta \neq 0,\ \pi$, C_{4z} symmetry is broken while C_{2z} is preserved. This means that around a vortex core, the system evolves continuously between two C_{4z} invariant insulators while keeping the C_{2z} symmetry. Fig. B.2 shows an example of the lattice structure modulation around the vortex. In real materials, since the $U(1)$ symmetry of the order parameter is reduced to a discrete C_n symmetry due to the lattice potential. An example of $\mathbb{Z}_4$ vortex structure is shown in Fig. B.2 (d) in which fractional charges are localized at the junction between four domains with $\theta = 0,\ \pi/4,\ \pi/2,\ 3\pi/4$, respectively [33, 41]. Here the four domains are obtained due to four different ways choosing the unit cell for given lattice structure.

$\mathcal{C}_{2z}\mathcal{T}$ symmetry.— Let us first consider spinless fermion systems. The low energy Dirac Hamiltonian describing a $C_{2z}T$ invariant insulator can be written as

$$H_D(\theta) = -i\Gamma_1\partial_1 - i\Gamma_2\partial_2 + M\cos\theta\Gamma_3 + M\sin\theta\Gamma_4, \tag{B.10}$$

where $\Gamma_1 = \tau_x$, $\Gamma_2 = \sigma_y\tau_y$, $\Gamma_3 = \tau_z$, $\Gamma_4 = \sigma_z\tau_y$, $\Gamma_5 = \sigma_x\tau_y$. Here we assume the following symmetry representations $C_{2z} = \Gamma_3 = \tau_z$, $T = \Gamma_3 K$, $C_{2z}T = K$

where K denotes complex conjugation. One can easily see that $H_D(\theta = 0,\ \pi)$ is $C_{2z}T$ invariant while $M \sin\theta\Gamma_4 \neq 0$ breaks C_{2z} and $C_{2z}T$ while keeping T invariance, and thus it can connect two $C_{2z}T$ invariant insulators with distinct topological properties.

The higher-order nature of $C_{2z}T$ invariant insulators can be seen by following the similar idea as in the case of C_{2z} symmetric systems. Namely, $H_D(\theta = 0,\ \pi)$ can be considered as two copies of quantum Hall insulators with opposite Chern numbers. Then after a suitable regularization, one can make $H_D(\theta = 0)$ to have a pair of counter-propagating chiral edge modes whereas $H_D(\theta = 0,\ \pi)$ has no edge state. By adding $C_{2z}T$ symmetric mass terms, corner charges can be found at the domain wall of the surface mass terms. Recently, it is shown that a $C_{2z}T$ invariant axion insulator, dubbed a 3D strong Stiefel Whitney insulator (SWI), can be described by using a pumping process between a 2D SWI and a trivial insulator with the corresponding Z_2 invariant $w_2 = 1$ and $w_2 = 0$, respectively. Also, it is shown that $w_2(k_z = 0) - w_2(k_z = \pi) \equiv 2P_3 \mod 2$ [9, 11].

In spinful fermion systems, one can use a different basis for symmetry representation. For instance, we can choose $C_{2z} = i\sigma_y$, $T = i\sigma_y K$, $C_{2z}T = K$, and also $\Gamma_1 = \sigma_x$, $\Gamma_2 = \sigma_z$, $\Gamma_3 = \sigma_y\tau_y$, $\Gamma_4 = \sigma_y\tau_x$, $\Gamma_5 = \sigma_y\tau_z$ where σ denotes the spin degrees of freedom. One can see that Γ_4 and Γ_5 terms break T symmetry while keeping C_{2z}. Hence the vortex structure breaks T when $\theta \neq 0,\ \pi$ in spinful fermion systems, whereas it breaks C_{2z} while keeping T in spinless fermion systems.

$\mathcal{C}_{4z}\mathcal{T}$ symmetry.— The low energy Dirac Hamiltonian describing a QSHI protected by C_{4z} and T is

$$H = -i\Gamma_1\partial_1 - i\Gamma_2\partial_2 + M\cos\theta\Gamma_3 + M\sin\theta\Gamma_4, \tag{B.11}$$

where $\Gamma_1 = \sigma_x\tau_x$, $\Gamma_2 = \sigma_y\tau_x$, $\Gamma_3 = \tau_z$, $\Gamma_4 = \sigma_z\tau_x$, $\Gamma_5 = \tau_y$, $C_4 = \cos(\pi/4) + \sin(\pi/4)\Gamma_1\Gamma_2$ and $T = i\sigma_y K$. Using $C_{4z}\Gamma_1 C_{4z}^{-1} = -\Gamma_2$, $C_{4z}\Gamma_2 C_{4z}^{-1} = \Gamma_1$, one can easily check the invariance of the Hamiltonian under C_{4z} and T. Also $\Gamma_4 = \sigma_z\tau_x$ and $\Gamma_5 = \tau_y$ break T but satisfy C_{4z}. Hence a constant mass term $M\sin\theta\Gamma_4 \neq 0$ describing a ferromagnetic ordering with out-of-plane magnetization, breaks T while keeping C_{4z}, and thus can connect two $C_{4z}T$ symmetric insulators with distinct topological properties.

The second order nature of the topological insulator protected by $C_{4z}T$ symmetry can be understood as follows. For convenience, let us consider a disk-shaped finite-size system with a circular boundary. We assume that $M > 0$ inside the insulator and $M < 0$ outside the insulator. In polar coordinates, the Hamiltonian is expressed as

$$H = -i\Gamma_1(\theta)\partial_r - i\Gamma_2(\theta)r^{-1}\partial_\theta + M(r)\Gamma_3, \tag{B.12}$$

where $\Gamma_1(\theta) = \cos\theta\Gamma_1 + \sin\theta\Gamma_2$ and $\Gamma_2 = -\sin\theta\Gamma_1 + \cos\theta\Gamma_2$. Employing a projection operator $P(\theta) = \frac{1}{2}(1 + i\Gamma_1(\theta)\Gamma_3)$, we get a gapless surface Hamiltonian $H|_{r=R} = -iR^{-1}\tilde{\sigma_z}\partial_\theta$, which is a characteristic of a QSHI. If T symmetry is broken but non-local C_4T symmetry is protected, surface mass terms are allowed: $H_m = m_4(\mathbf{r})\Gamma_4 + m_5(\mathbf{r})\Gamma_5$. Projection to the surface gives $H_m|_{r=R} = m_4\tilde{\sigma_x} + m_5\tilde{\sigma_y}$. Under C_4T symmetry, mass terms change sign: $m_i(\mathbf{r}) = -m_i(C_4\mathbf{r})$. Since two masses do not vanish simultaneously in general, the system does not exhibit anomalous corner states. However, in the presence of chiral symmetry, for instance, $\Gamma_5 H\Gamma_5^{-1} = -H$, m_5 must vanish, so that C_{4z} symmetric corner states appear.

The corresponding lattice Hamiltonian describing a C_4T invariant axion

insulator is proposed in Ref. [38] as

$$H(\mathbf{k}) = (M + t\sum_i \cos k_i)\tau_z\sigma_0 + \Delta_1 \sum_i \sin k_i \tau_x \sigma_i + \Delta_2(\cos k_x - \cos k_y)\tau_y\sigma_0 \tag{B.13}$$

where $-3 < M/t < -1$. Between $k_z = 0$ and π, mass term changes sign, which means that one of them describes a second order topological insulator and the other is a trivial insulator. Thus, the axion insulator exhibits a pumping process between a 2D chiral symmetric second order topological insulator and a trivial insulator. Similar to the case with $\mathcal{T}$ symmetry, $(\mathcal{C}_{4z}\mathcal{T})^4 = -1$ condition is crucial to define an axion insulator phase. For instance, let us suppose that there is $\mathcal{C}_{4z}\mathcal{T}$ symmetric chiral hinge modes for a finite size system. On the top surface, there must be gapless modes that respect $\mathcal{C}_{4z}\mathcal{T}$ symmetry. However, gapless modes are not protected for spinless fermion systems. Whereas gapless modes are protected for spinful electron systems since $+i$ and $-i$ eigenvalues of $\mathcal{C}_{2z}$ symmetry are always paired due to $\mathcal{C}_{4z}\mathcal{T}$ symmetry.

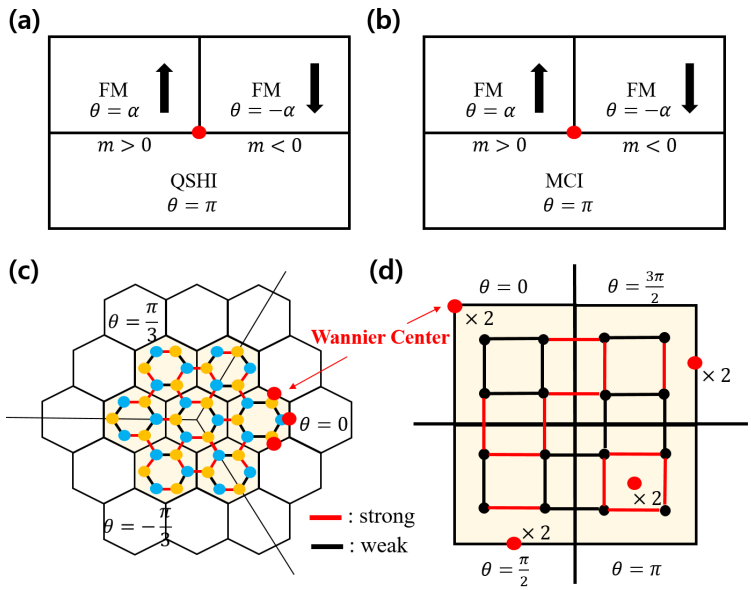

Figure B.1 (Color online) (a) A heterostructure where fractional charges are bound at the junction between a QSHI ($\theta = 0$) and two ferromagnetic insulators (FM, $\theta = \pm\alpha$) with opposite in-plane magnetization. Since two FMs introduce surface mass terms with opposite sign, a zero-mode state is localized at the junction. (b) Similar heterostructure for a mirror Chern insulator. (c) A $\mathbb{Z}_3$ vortex of Kekule textured graphene where three domains with lattice structure $\theta = 0$, $\pi/3$, $-\pi/3$ meet at a junction. Due to the Wannier function centered at the unit cell boundary at $\theta = 0$, the vortex geometry contains half-integer electrons. (d) A $\mathbb{Z}_4$ vortex relevant to C_{4z} symmetric insulators with a quantized quadrupole moment where four domains with lattice structure $\theta = 0$, $\pi/2$, π, and $3\pi/2$ meet at a junction. Due to the Wannier functions centered at the unit cell corner at $\theta = 0$, half-integer electrons are bound to the vortex center.

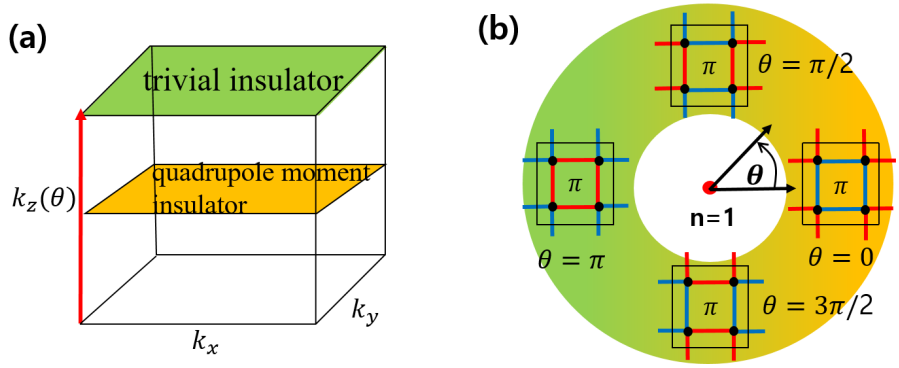

Figure B.2 (Color online) (a) Schematic figure describing the lattice structure around a vortex in a C_{4z} invariant insulator. (b) Schematic figure describing the $\mathcal{C}_{4z}\mathcal{P}$ symmetric axion insulator in momentum space. Here the $k_z(\theta) = 0$ plane corresponds to the $2D$ insulator with a quantized quadrupole moment while the $k_z(\theta) = \pi$ plane corresponds to a trivial insulator.

Appendix C

Wannier center and quantized fractional charge in topological vortex

Here we use symmetric Wannier function description to show that fractional charge bound to a topological vortex is quantized even without chiral or particle-hole symmetry. Let us first consider a 1D domain wall system of SSH Hamiltonian. The value of polarization should be quantized into 0 or 1/2 mod 1 in the presence of inversion symmetry. When $P = 0$, Wannier function is located at the center of the unit cell. In the case of $P = 1/2$, on the other hand, Wannier function is located at the unit cell boundary. Fig. C.1 (a) describes the domain wall structure of SSH Hamiltonian between trivial and topological phases. On the left side($P = 0$), Wannier center is located at the unit cell center. On the other side($P = 1/2$), Wannier center is located at the unit cell boundary, where two adjacent cells share the electron located at the cell boundary: the electron gives half charge contribution to each unit cell. There-

fore, the domain structure composed of integer unit cells contains half-integer electrons due to the electron located at the unit cell boundary at the right side. It shows that the inversion symmetry keeps half-integer charge localized at the domain wall of the SSH chain.

Similarly, the half-quantized charge bound to a topological vortex can be explained by the Wannier function description. Except for T and M_z, there are four symmetries $P(C_{2z}), C_{2z}T, C_{4z}$, and $C_{4z}T$ that are relevant to the vortices with higher-order topology. Since T is local-in-space symmetry, it does not change the position of Wannier center. Thus, to prove that half-integer charge is bound to topological vortex, we only have to consider P (or C_{2z}) and C_{4z} symmetries.

P (or C_{2z}).— Inversion symmetric insulator has four Wyckoff positions A,B,C, and D which are invariant under inversion up to lattice translation vector (Fig. C.1 (a)). We define the number of symmetric Wannier functions centered at each Wyckoff position as N_A, N_B, N_C, and N_D. For inversion symmetric HOTI, polarization is zero:

$$p_x = \sum_i X_i = \frac{1}{2}(N_B + N_C) = 0 \mod 1, \tag{C.1}$$

$$p_y = \sum_i Y_i = \frac{1}{2}(N_C + N_D) = 0 \mod 1 \tag{C.2}$$

where X_i and Y_i denote x and y coordinates of ith Wannier function, respectively. On the other hand, quadrupole moment is defined as

$$q_{xy} = \sum_i X_i Y_i = \frac{1}{4}N_C = \frac{1}{4} \mod \frac{1}{2}. \tag{C.3}$$

Let us note that N_C is well defined modulo 2 since N_C can be changed only by multiples of two keeping inversion symmetry. Taken altogether, $N_B = N_C = N_D = 1 \mod 2$. For a trivial insulator, on the other hand, quadrupole moment $q_{xy} = \frac{1}{4}N_C = 0 \mod \frac{1}{2}$ Thus, $N_B = N_C = N_D = 0 \mod 2$. Let us consider a

vortex structure $PH(k_x, k_y, \theta)P^{-1} = H(-k_x, -k_y, -\theta)$ where $\theta = 0(\pi)$ corresponds to inversion symmetric HOTI (trivial insulator) (Fig. C.1 (c)). Since odd number of Wannier functions are located at the unit-cell boundary for $\theta = 0$, the vortex geometry composed of integer unit-cells contains half-integer charge. Let us note that the half-integer charge only comes from $\theta = 0$ since even if an electron is located at the cell boundary at arbitrary $\theta \neq 0$, another electron should be located at the cell boundary at $-\theta$ due to the relation $PH(\mathbf{k}, \theta)P^{-1} = H(-\mathbf{k}, -\theta)$.

C_{4z}.— C_{4z} symmetric insulator has two Wyckoff positions A and C which are invariant under C_{4z} operation and two Wyckoff positions B and D which are invariant under C_{2z} operation up to lattice translation vector (Fig. C.1 (b)). The vortex structure satisfies $C_{4z}H(k_x, k_y, \theta)C_{4z}^{-1} = H(k'_x, k'_y, -\theta)$, followed by $C_{2z}H(k_x, k_y, \theta)C_{2z}^{-1} = H(-k_x, -k_y, \theta)$. Since we are not interested in inversion symmetry protected topological phase, $N_B = N_C = N_D = 0 \mod 2$ for any θ. As shown earlier, in the case of C_{4z} symmetric HOTI, $N_C = 2 \mod 4$. Also, $N_C = 0 \mod 4$ for trivial insulator. Note that N_C is well defined modulo 4 since N_C can be changed by multiples of four keeping C_4 symmetry. The charge bound to the vortex is, therefore, $\frac{1}{4}(N_C(\theta = 0) + N_c(\theta = \pi)) = \frac{1}{2} \mod 1$, for the electron located at the Wyckoff position C gives 1/4 charge contribution to each unit cell (Fig. C.1 (d)).

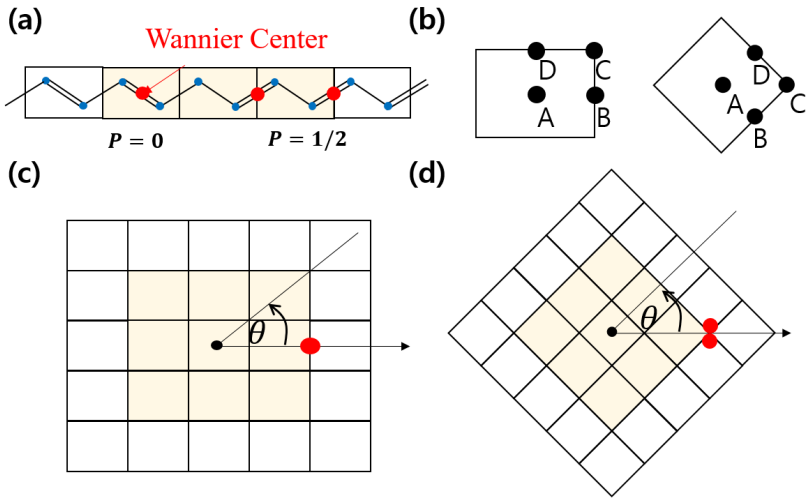

Figure C.1 (Color online) (a) Domain wall structure between trivial ($P = 0$) and topological($P = 1/2$) insulator. Since Wannier function is located at the unit cell boundary for $P = 1/2$, the domain wall structure composed of integer unit cells (shaded region) contains half integer electrons. (b) Wycoff positions of P and C_{4z} symmetric lattices. (c) Topological vortex protected by inversion symmetry. For $\theta = 0$(inversion symmetric HOTI), $N_B = N_C = N_D = 1 \mod 2$. Since Wannier function is located at the unit cell boundary at $\theta = 0$, the charge bound to the vortex is quantized into half-integer. (d) Topological vortex protected by C_{4z} symmetry. Since $N_C(\theta = 0) = 2 \mod 4$ (C_{4z} symmetric HOTI), the charge bound to the vortex is $\frac{1}{4}(2N_C(\theta = 0) + 2N_c(\theta = \pi)) = \frac{1}{2} \mod 1$

Bibliography

[1] W.-P. Su, J. Schrieffer and A. Heeger, *Soliton excitations in polyacetylene*, *Physical Review B* **22** (1980) 2099.

[2] T. L. Hughes, E. Prodan and B. A. Bernevig, *Inversion-symmetric topological insulators*, *Physical Review B* **83** (2011) 245132.

[3] A. M. Turner, Y. Zhang, R. S. Mong and A. Vishwanath, *Quantized response and topology of magnetic insulators with inversion symmetry*, *Physical Review B* **85** (2012) 165120.

[4] X.-L. Qi, T. L. Hughes and S.-C. Zhang, *Topological field theory of time-reversal invariant insulators*, *Physical Review B* **78** (2008) 195424.

[5] B. A. Bernevig and S.-C. Zhang, *Quantum spin hall effect*, *Physical review letters* **96** (2006) 106802.

[6] J. Ahn, D. Kim, Y. Kim and B.-J. Yang, *Band topology and linking structure of nodal line semimetals with Z_2 monopole charges*, *Physical Review Letters* **121** (2018) 106403.

[7] J. Zak, *Berry's phase for energy bands in solids*, *Physical Review Letters* **62** (1989) 2747.

[8] D. Xiao, M.-C. Chang and Q. Niu, *Berry phase effects on electronic properties*, *Reviews of Modern Physics* **82** (2010) 1959.

[9] J. Ahn and B.-J. Yang, *Symmetry representation approach to topological invariants in $c_{2z}t$-symmetric systems*, *Physical Review B* **99** (2019) 235125.

[10] J. Ahn, S. Park and B.-J. Yang, *Failure of nielsen-ninomiya theorem and fragile topology in two-dimensional systems with space-time inversion symmetry: application to twisted bilayer graphene at magic angle*, *Physical Review X* **9** (2019) 021013.

[11] B. J. Wieder and B. A. Bernevig, *The axion insulator as a pump of fragile topology*, *Preprint at http://arXiv.org/abs/1810.02373* (2018) .

[12] Z. Song, T. Zhang and C. Fang, *Diagnosis for nonmagnetic topological semimetals in the absence of spin-orbital coupling*, *Physical Review X* **8** (2018) 031069.

[13] L. Fu and C. L. Kane, *Topological insulators with inversion symmetry*, *Physical Review B* **76** (2007) 045302.

[14] Y. Kim, B. J. Wieder, C. Kane and A. M. Rappe, *Dirac line nodes in inversion-symmetric crystals*, *Physical Review Letters* **115** (2015) 036806.

[15] H. C. Po, A. Vishwanath and H. Watanabe, *Symmetry-based indicators of band topology in the 230 space groups*, *Nature Communications* **8** (2017) 50.

[16] C.-Y. Hou, C. Chamon and C. Mudry, *Electron fractionalization in two-dimensional graphenelike structures*, *Physical review letters* **98** (2007) 186809.

[17] M. M. Haley, S. C. Brand and J. J. Pak, *Carbon networks based on dehydrobenzoannulenes: synthesis of graphdiyne substructures*, *Angewandte Chemie International Edition in English* **36** (1997) 836.

[18] G. Li, Y. Li, H. Liu, Y. Guo, Y. Li and D. Zhu, *Architecture of graphdiyne nanoscale films*, *Chemical Communications* **46** (2010) 3256.

[19] Y. Zhao and Y. Lu, *pt-symmetric real dirac fermions and semimetals*, *Physical Review Letters* **118** (2017) 056401.

[20] C. Fang, Y. Chen, H.-Y. Kee and L. Fu, *Topological nodal line semimetals with and without spin-orbital coupling*, *Physical Review B* **92** (2015) 081201.

[21] *See Appendix for details* .

[22] Z. Wang, B. J. Wieder, J. Li, B. Yan and B. A. Bernevig, *Higher-order topology, monopole nodal lines, and the origin of large fermi arcs in transition metal dichalcogenides XTe_2 (X= Mo, W)*, *Physical Review Letters* **123** (2019) 186401.

[23] W. A. Benalcazar, B. A. Bernevig and T. L. Hughes, *Quantized electric multipole insulators*, *Science* **357** (2017) 61.

[24] W. A. Benalcazar, T. Li and T. L. Hughes, *Quantization of fractional corner charge in c_n-symmetric higher-order topological crystalline insulators*, *Physical Review B* **99** (2019) 245151.

[25] T. Nomura, T. Habe, R. Sakamoto and M. Koshino, *Three-dimensional graphdiyne as a topological nodal-line semimetal*, *Physical Review Materials* **2** (2018) 054204.

[26] R. Jackiw and C. Rebbi, *Solitons with fermion number* 1/2, *Physical Review D* **13** (1976) 3398.

[27] R. Jackiw and P. Rossi, *Zero modes of the vortex-fermion system*, *Nuclear Physics B* **190** (1981) 681.

[28] J. Goldstone and F. Wilczek, *Fractional quantum numbers on solitons*, *Physical Review Letters* **47** (1981) 986.

[29] N. Read and D. Green, *Paired states of fermions in two dimensions with breaking of parity and time-reversal symmetries and the fractional quantum hall effect*, *Physical Review B* **61** (2000) 10267.

[30] J. C. Teo and C. L. Kane, *Majorana fermions and non-abelian statistics in three dimensions*, *Physical review letters* **104** (2010) 046401.

[31] J. C. Teo and C. L. Kane, *Topological defects and gapless modes in insulators and superconductors*, *Physical Review B* **82** (2010) 115120.

[32] C. Chamon, C.-Y. Hou, R. Jackiw, C. Mudry, S.-Y. Pi and G. Semenoff, *Electron fractionalization for two-dimensional dirac fermions*, *Physical Review B* **77** (2008) 235431.

[33] C. Chamon, C.-Y. Hou, R. Jackiw, C. Mudry, S.-Y. Pi and A. P. Schnyder, *Irrational versus rational charge and statistics in two-dimensional quantum systems*, *Physical review letters* **100** (2008) 110405.

[34] S. Ryu, C. Mudry, C.-Y. Hou and C. Chamon, *Masses in graphenelike two-dimensional electronic systems: Topological defects in order parameters and their fractional exchange statistics*, *Physical Review B* **80** (2009) 205319.

[35] D. Varjas, F. de Juan and Y.-M. Lu, *Bulk invariants and topological response in insulators and superconductors with nonsymmorphic symmetries*, *Physical Review B* **92** (2015) 195116.

[36] F. Schindler, Z. Wang, M. G. Vergniory, A. M. Cook, A. Murani, S. Sengupta et al., *Higher-order topology in bismuth*, *Nature Physics* **14** (2018) 918.

[37] G. Van Miert and C. Ortix, *Higher-order topological insulators protected by inversion and rotoinversion symmetries*, *Physical Review B* **98** (2018) 081110.

[38] F. Schindler, A. M. Cook, M. G. Vergniory, Z. Wang, S. S. Parkin, B. A. Bernevig et al., *Higher-order topological insulators*, *Science Advances* **4** (2018) eaat0346.

[39] E. Khalaf, H. C. Po, A. Vishwanath and H. Watanabe, *Symmetry indicators and anomalous surface states of topological crystalline insulators*, *Physical Review X* **8** (2018) 031070.

[40] D. L. Bergman, *Realization of a vortex in the kekule texture of molecular graphene at a y junction where three domains meet*, *Physical Review B* **87** (2013) 035422.

[41] W. A. Benalcazar, B. A. Bernevig and T. L. Hughes, *Electric multipole moments, topological multipole moment pumping, and chiral hinge states in crystalline insulators*, *Physical Review B* **96** (2017) 245115.

[42] B.-Y. Xie, H.-F. Wang, H.-X. Wang, X.-Y. Zhu, J.-H. Jiang, M.-H. Lu et al., *Second-order photonic topological insulator with corner states*, *Physical Review B* **98** (2018) 205147.

[43] L. Fu and C. L. Kane, *Time reversal polarization and a z 2 adiabatic spin pump*, *Physical Review B* **74** (2006) 195312.

[44] S. Ryu, A. P. Schnyder, A. Furusaki and A. W. Ludwig, *Topological insulators and superconductors: tenfold way and dimensional hierarchy*, *New Journal of Physics* **12** (2010) 065010.

[45] X.-L. Qi, T. L. Hughes and S.-C. Zhang, *Fractional charge and quantized current in the quantum spin hall state*, *Nature Physics* **4** (2008) 273.

[46] J. C. Teo, L. Fu and C. Kane, *Surface states and topological invariants in three-dimensional topological insulators: Application to bi 1- x sb x*, *Physical Review B* **78** (2008) 045426.

[47] E. Khalaf, *Higher-order topological insulators and superconductors protected by inversion symmetry*, *Physical Review B* **97** (2018) 205136.

초록

벌크-경계 대응성은 위상학적 물질이 가지고 있는 기본 성질이다. 전통적인 위상학적 절연체에서, d 차원의 절연물질은 $(d-1)$차원 표면에서 금속 상태를 가진다. 하지만 최근에 이러한 벌크-경계 대응성을 깨는 위상학적 결정 절연체의 존재가 소개되었으며 이는 고차 위상 절연체라고 불린다. 전통적인 위상학적 절연체와는 다르게 d차원 고차 위상 절연체는 물질의 전체적인 모양이 벌크 띠 위상과 관련된 결정 대칭을 유지될 때 $(d-1)$차원 보다 작은 차원의 부분공간인 경첩이나 모서리에 금속 상태가 국한 되어 있다. 이 논문에서, 우리는 결정 대칭에 의해 보호되는 2차원 고차 위상 절연체에 나타날 수 있는 새로운 특성을 조사한다.

먼저, 우리는 케쿨레 그래핀의 띠 위상이 반전 대칭 시스템에서 양자화되는 $\mathbb{Z}_2$ 위상 불변 w_2를 특징으로하는 2차원 고차 위상 절연체임을 보였다. 또한, 케쿨레 그래핀과 동일한 결정 대칭을 갖는 반전 대칭에 의해 보호되는 2차원 고차 위상 절연체에 대한 최초의 현실적인 후보 물질로서 단일 층 그래프다인을 제안한다. 카이랄 대칭의 부재에도 불구하고, 단일 층 그래프다인의 고차 위상은 채움 아노말리로 나타난다. 흥미롭게도, 에너지 전자 성질은 p_z 오비탈 기반만을 사용하여 올바르게 설명 할 수 있지만, 고차 위상 자체는 중심부 전자 오비탈에서 비롯된다. 우리는 또한 단층 그래프다인의 고차 위상이 홀극 마디선과 힌지 상태를 가지는 ABC 그래프다인 띠 위상의 근원임을 보여준다.

두번째로, 우리는 격자 소용돌이에 구속된 분수 전하와 2차원 고차 위상 절연체의 벌크 띠 위상이 대응됨을 보인다. Su-Schrieffer-Heeger 모델의 구역 벽에 분수 전하가 국한된 것이 전하 분극의 차이에 의해 나타나는 것 처럼 케쿨레 격자의 소용돌이에 국한된 부분 전하는 소용돌이 주위의 벌크 위상 불변 w_2의 변화와 관련이있는 것으로 나타난다. 또한 케쿨레 그래핀에서 소용돌이 주위의 각도 θ를 세번째 좌표로 나타냈을 때 만들어진 3차원 해밀토니안은 양자화 된 자기 전기 분극을 갖는 삼차 액시온 절연체을 설명한다. 시공간 방향을 반전시키는 대칭의

존재로 인해 액시온 절연체가 만들어지는 경우에, 우리는 소용돌이가 부분 전하를 갖는 모든 가능한 위상 결정 절연체를 분류한다.

주요어: 고차 위상, 결정 대칭, 단층 그래프다인, 위상학적 소용돌이
학번: 2017-24557